Background

Cell cycle checkpoint is the mechanism that secures integrity of the genome. It is activated by DNA damage caused by DNA damaging agents, such as ionizing radiation [1]. Activated checkpoints halt cell cycle progression or execute cell death. Three major cell cycle checkpoints induced by IR include G1 checkpoint preventing G1-S transition, intra-S checkpoint halting DNA replication, and G2/M checkpoint that inhibits G2 cells to enter mitosis [2]. The master regulator of the IR-induced cell cycle checkpoints is ataxia telangiectasia mutated (ATM) protein, a serine/threonine kinase which belongs to a phospho-inositide 3-kinase (PI3K)-related kinase family [3]. ATM protein form inactive dimers or higher-order multimers in unstressed cells, but it is activated through intermolecular autophosphorylation at Ser1981 and monomerization in response to alteration of chromatin structure induced by DNA double-strand breaks or other chromatin-perturbing treatments [4]. A recent proteomic study revealed that, in response to IR, ATM phosphorylates > 900 serine and/or threonine residues on > 700 proteins including factors involved in cell cycle checkpoints, such as Chk2 and p53 [5], and, thus, ATM transactivates DNA damage checkpoints. In G2/M checkpoint, ATM activates Chk2 through phosphorylation at Thr68 [6,7]. Then, activated Chk2 phosphorylates and negatively regulates CDC25C, which is the positive regulators for the activity of cdc2/cyclinB required for mitosis entry [8].

Recently, phosphorylated forms of such downstream factors have been treated as surrogate markers for DNA damage signaling. For example, several studies unraveled that histone H2AX, which is a subtype of histone H2A, and constitutes 2-25% of total H2A protein, was phosphorylated at Ser139 by ATM in response to DSBs. Phosphorylation of histone H2AX spans several mega base pairs of chromatin flanking DSBs [9-12], and thus, phosphorylated histone H2AX can be microscopically visible as nuclear foci by immunofluorescence staining using specific antibody recognizing phosphorylated forms of histone H2AX [13]. It is now generally considered that a focus of phosphorylated H2AX, also called as gamma-H2AX focus, represents a single DSB, because the number of foci per cell immediately after IR is very close to theoretically-estimated DSB number after given doses of IR [13]. Thus, phosphorylated H2AX foci are now widely used as an indicator for DSBs [14]. However, more recent studies also revealed that phosphorylated H2AX foci is not just an indicator for DSBs, but also a platform playing an essential role in DNA damage signaling. It was reported that a number of other proteins also form the colocalized foci with phosphorylated H2AX foci, whose colocalization was totally relied on H2AX phosphorylation. Such proteins include MDC1, 53BP1, RNF8, MRE11-Rad50-NBS1 complex [4,15-24]. Moreover, these foci-forming proteins are critical for accumulation of phosphorylated ATM at focal site, and therefore, they are considered to be involved in ATM-dependent DSB response [25-27]. Indeed, depletion of H2AX phosphorylation or colocalized factors negatively affects IR-induced checkpoint, especially, in cells exposed to lower doses of IR [17,21,24,28,29].

We previously demonstrated that persistent Ser1981-phosphorylated ATM foci grow in size after IR, and the foci size of the phosphorylated ATM is well correlated with phosphorylation levels of p53 at serine15, which is the direct target of ATM. It is indicated that foci growth could be an essential mechanism for amplifying the DNA damage signal for G1 checkpoint activation [30]. Otherwise, inappropriate DNA damage amplification fails in executing G1 arrest, as shown in AT and NBS cells [30]. While the DNA damage signal amplification is indispensable for G1 arrest, a role of amplification of DNA damage signal in G2 checkpoint activation remains to be determined.

In the present study, we developed a novel quantitative parameter for DNA damage signal. Because the number of foci is well correlated with the number of DSBs but the foci number might not be an appropriate index for the amount of DNA damage signal, our parameter integrates not only the number but also the size of IR-induced foci for proper quantification of DNA damage signal. The new parameter, SOID, represents the sum of fluorescence of each focus within one nucleus. The SOID was calculated for individual nucleus as the sum of (area (total pixel numbers) of each focus) x (mean fluorescence intensity per pixel of each focus), and it was expected to reflect the flux of DNA damage signal much more accurately than foci number. We performed a "two-way" comparison of SOID of Ser139-phosphorylated histone H2AX foci between G2-arrested cells and mitosis-progressing cells. The analysis revealed that there was a threshold of DNA damage signal for G2 arrest, which was around 4000~5000 SOID. Chromosome analysis revealed that the checkpoint-neglected mitosis-progressing cells had approximately two chromatid breaks on average, indicating that 4000~5000 SOID was equivalent to a few DNA double strand breaks.

Results

Quantification of DNA damage signal involved in G2/M checkpoint activation

To quantify DNA damage signal sufficient for G2 arrest we compared the amount of DNA damage signal

detected in G2-arrested cells with that in mitosis-progressing cells after IR. For this purpose, we decided to use very low doses of X-rays (0.02~0.4 Gy). Because higher doses of X-rays, such as 1 Gy, completely arrested G2 cells in our normal human primary fibroblasts, it prevented examination of signal amount left in mitosis-progressing cells. For example, no mitotic cells were observed in 7440 cells analyzed 2 hr after 1 Gy. We also quantified DNA damage signal in mitosis-progressing cells exposed to IR in the presence of inhibitors for ATM or Chk1/2, which enabled G2 to mitosis progression irrespective of the amount of DNA damage signal. For quantification of DNA damage signal, we used the foci of Ser139-phosphorylated histone H2AX. The size of phosphorylated H2AX foci well correlated with that of Ser1981-phosphorylated ATM foci, and phosphoryated H2AX foci could be detectable in mitotic cells [31]. This was in contrast to the other DNA damage checkpoint factors like 53BP1, which were not detectable in mitosis [32].

First, we examined the mitotic index 2 hr after irradiation with 0.02, 0.04, 0.08, 0.1, 0.2, and 0.4 Gy of X-rays in the presence or absence of KU55933 (10 μM) or SB218078 (2.5 μM), which is well-established inhibitor for ATM and Chk1/2, respectively [33,34]. Mitotic cells were identified by immunofluorescence staining of Ser10-phosphorylated histone H3. The mitotic index was decreased dose-dependently in the absence of the inhibitors, indicating that G2 arrest was efficiently induced even by low doses of X-rays (Figure 1). We found that G2 arrest was largely dependent on ATM-dependent chk2 activation, as it was almost abrogated in the presence of KU55933 or SB218078 even after 0.4 Gy (Figure 1). Next, we compared the number of phosphorylated H2AX foci between G2 cells and mitotic cells 2 hr after X-irradiation. G2 cells were distinguished from mitotic cells by weaker intensity and more rugged and discontinuous pattern of phosphorylated histone H3 staining. Representative photos presented in Figure 2 showed that the number of foci in mitosis-progressing cells was not always less than that observed in G2 cells. However, we noted that the size of the foci was much smaller in mitosis-progressing cells. Dose-dependent induction of foci in G2 and mitotic cells, shown in Figure 3, also indicated that there was no apparent difference in the foci numbers between G2 cells and mitotic cells. For example, similar foci numbers were observed in G2 and mitotic cells exposed to 0.4 Gy of X-rays, whose dose clearly induced G2 arrest in substantial proportion of cells (Figure 1). Because the weaker fluorescence intensity was commonly observed in the foci of mitosis-progressing cells, it was indicated that the size of foci in addition to the foci number should be taken into consideration, when the amount of DNA damage

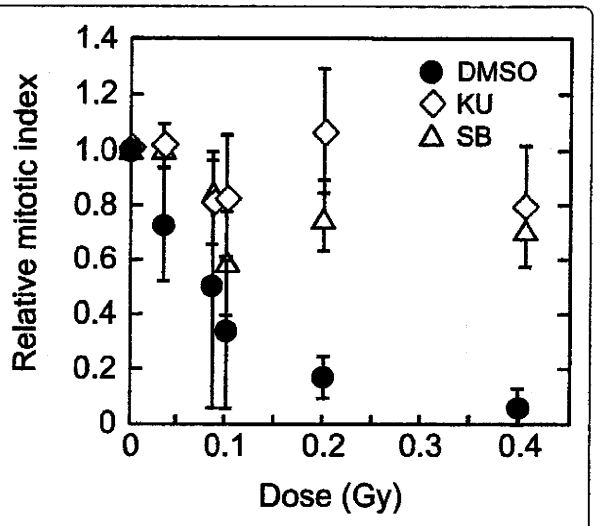

Figure 1 G2 arrest and its inhibition induced by low doses of X-rays. Exponentially-growing normal human primary fibroblasts were irradiated with 0, 0.02, 0.04, 0.08, 0.1, 0.2, and 0.4 Gy of X-rays, and two hours later, cells were fixed and subjected to immunofluorescence staining for Ser10-phosphorylated histone H3. KU55933 (10 μM), SB218078 (2.5 μM), or their solvent DMSO was administrated 30 min before IR. Mitotic cells were identified by strong fluorescence intensity of phosphorylated H3 signals. More than 5000 cells were scored at each dose and each treatment, and the results obtained from three independent experiments were pooled. Data indicate mean ± SD.

signal was evaluated based upon the foci. Therefore, we invented a novel parameter, into which the foci number, the foci size, and fluorescence intensity of each focus were all integrated.

The new parameter was designated as SOID, which represents the sum of fluorescence of each focus within one nucleus. The SOID was calculated for individual nucleus as the sum of (area (total pixel numbers) of each focus) x (mean fluorescence intensity per pixel of each focus). As shown in Figure 4, SOID values were calculated for each nucleus. For example, the numbers of foci in I and II nuclei are 12 and 9, respectively, whereas the SOID values are calculated as 7092 and 3148. The relationship between the SOID values and the numbers of foci was examined in cells exposed to 0.4 Gy of X-rays (Figure 5). We observed no close relation between the numbers and the SOID values by linear regression analysis (correlation coefficient R = 0.68), confirming that the foci numbers alone were insufficient for evaluating the amount of DNA damage signal. Then, dose-dependent increase in the SOID values is determined 2 hours after 0.4 Gy of X-rays (Figure 6). At this time point, the number of foci was approximately a half of that of the foci initially formed, according to DNA repair. Some of the foci became smaller, while the persisted foci tended to grow. Therefore, the amount of

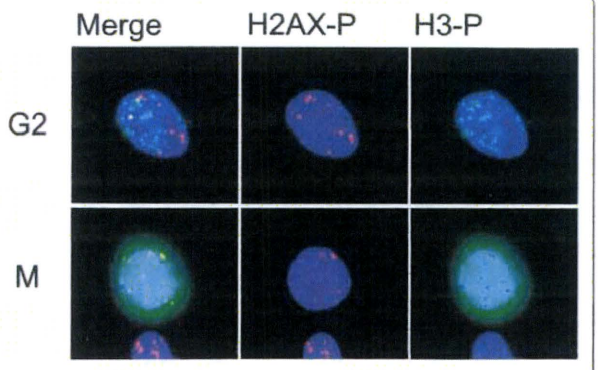

Figure 2 Phosphorylated histone H2AX foci formed in G2 and mitotic cells. Formation of phosphorylated H2AX foci and phosphorylation of histone H3 were examined in G2 cells and mitotic cells 2 hr after 0.4 Gy of X-rays. Note that G2 cells have weaker intensity and more rugged and discontinuous pattern of phosphorylated histone H3 staining compared to mitotic cells. In contrast, mitotic cells have foci with smaller size and weaker fluorescence intensity than G2 cells.

fluorescence of each focus was quite different. As a result, the SOID values showed large deviation, but we observed a tendency of dose-dependent increase above 0.1 Gy.

Threshold of SOID for G2 arrest

In order to determine a threshold for G2 arrest, we performed a "two-way" comparison of the SOID. Namely,

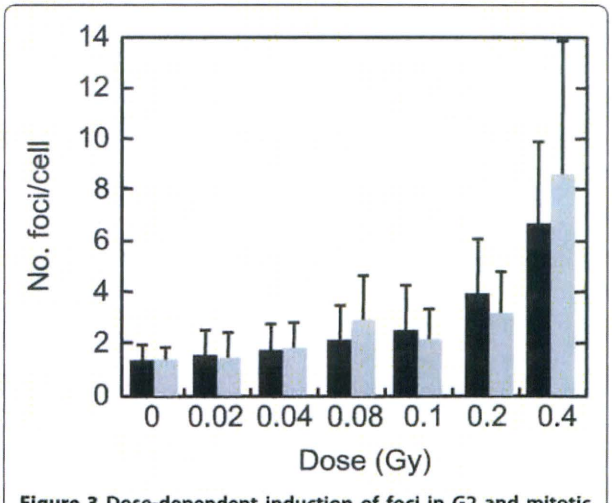

Figure 3 Dose-dependent induction of foci in G2 and mitotic cells. Exponentially-growing normal human primary fibroblasts were irradiated with 0, 0.02, 0.04, 0.08, 0.1, 0.2, and 0.4 Gy of X-rays, and two hours later, cells were fixed and subjected to immunofluorescence staining for Ser139-phosphorylated H2AX and Ser10-phosphorylated H3. Foci numbers of Ser139-phosphorylated histone H2AX in G2 cells and mitotic cells were counted. G2 cells (black bars) and mitotic cells (grey bars) were identified as described in Figure 2. Data indicate means ± SD.

Figure 4 Representative SOID measurements in G2 cells. The SOID values were examined in cells 2 hours after exposure to 0.4 Gy of X-rays. The SOID was measured as described in Methods. Left panel: the SOID values in each nucleus. Right panel: white arrows indicate two nuclei with similar foci numbers but different the SOID values.

one is between G2-arrested cells and mitosis-progressing cells, and the other is between mitotic cells cultured after X-irradiation in the presence or absence of G2/M checkpoint inhibitors. Exponentially-growing normal human primary fibroblasts were irradiated with 0.4 Gy of X-rays and fixed at 2 hr after IR. The inhibitors or their solvent DMSO was administrated 30 min before IR until 30 minutes before the time of sample preparation. Because KU55933 by itself affected the foci formation of phosphorylated histone H2AX, it was washed out 30 min before fixation to recover size and fluorescence intensity of the foci.

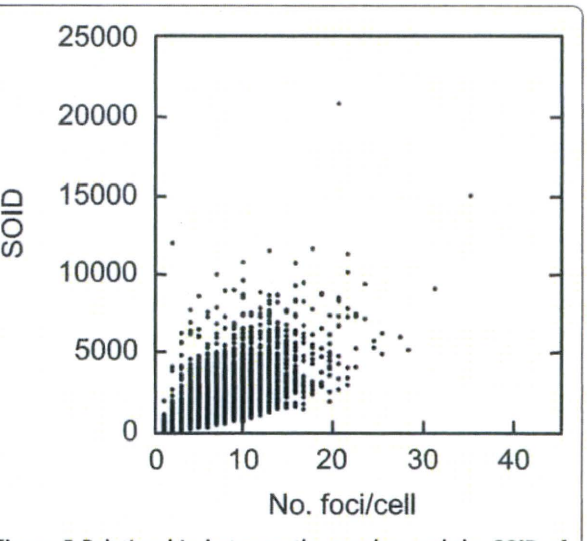

Figure 5 Relationship between the number and the SOID of foci per cell. Exponentially-growing normal human primary fibroblasts were irradiated with 0.4 Gy of X-rays, and two hours later, cells were fixed and subjected to immunofluorescence staining for Ser139-phosphorylated H2AX and Ser10-phosphorylated H3. The SOID values and the number of foci were examined in G2 cells. The SOID was measured as described in Methods. The SOID values and the corresponding foci numbers were plotted.

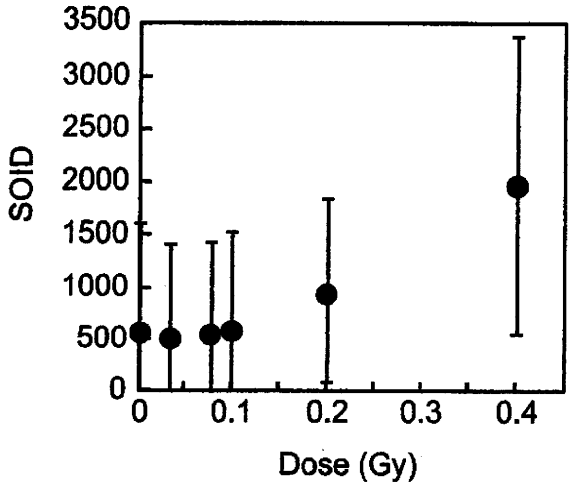

Figure 6 Dose-dependent increase of the SOID in G2 cells. Exponentially-growing normal human primary fibroblasts were irradiated with 0, 0.02, 0.04, 0.08, 0.1, 0.2, and 0.4 Gy of X-rays, and two hours later, cells were fixed and subjected to immunofluorescence staining for Ser139-phosphorylated H2AX and Ser10-phosphorylated H3. The SOID values were examined in G2 cells. The SOID was measured as described in Methods. Data indicate means ± SD.

A clear difference in the SOID distribution was observed at 0.4 Gy. The SOID values spanned between 0 to 6000 in 0.4 Gy-irradiated G2 cells (Figure 7B), however, mitotic cells with > 4000 SOID were rarely observed after 0.4 Gy (Figure 7D). We found that 7% of cells showed the SOID over 4000 in G2 cells but not in mitosis-progressing cells. This result suggested that cells with > 4000 SOID were unable to enter mitosis. Therefore, we confirm this with cells exposed to 1.0 Gy of X-rays. As 1.0 Gy of X-rays induced G2 arrest, no mitotic cells were detected 2 hours after X-irradiation (Figure 7G). In G2 cells, we found the SOID values expanding for over 15000 (Figure 7E). Since we found cells released from G2 arrest after 6 hours, the samples were prepared at 6, 8 and 12 hours after X-irradiation. The compiled data showed that 6% of G2 cells had the SOID over 4000 (Figure 7F), whereas that of mitotic cells was below 4000 (Figure 7H). Then, the SOID was compared between G2 cells and mitosis-progressing cells exposed to 0.4 Gy of X-rays in the presence or absence of the inhibitors. The SOID value in mitosis-progressing cells is significantly lower than that of G2 cells, while they are not very different when ATM activity is inhibited (Figure 8). In cells treated with KU55933 or SB218078, the SOID value spanned 0 - 7000 and 0 - 8000 in mitosis-progressing cells, respectively (Figures 9D and 9H), and we confirmed the SOID distribution was not significantly varied between G2 and mitotic cells. Thus, it was confirmed that G2 cells with > 4000 SOID was restricted to progress into mitosis in the presence of G2/M checkpoint. While most of the mitosis-progressing cells showed SOID value not more than 3000, there were very few but some mitosis-progressing cells with more than 3000 SOID. Therefore, we concluded that the threshold of SOID value for G2 arrest was estimated to be between 4000~5000.

Relationship between SOID value and the number of chromomatid breaks

As the threshold of SOID value for G2 arrest was estimated to be between 4000~5000, we then asked what is the cytological damage corresponding to 4000~5000 SOID. We analyzed chromatid breaks in mitosis-progressing cells 2 hr after 0.02-0.4 Gy of X-rays (Figure 10). Colcemid (0.1 μg/ml) was treated from immediately after IR to 2 hr after IR to collect metaphase cells. Here, we again used KU55933 to inhibit G2/M checkpoint. To make experimental setting consistent with the SOID analysis, KU55933 was washed out 30 min before metaphase harvest. We found the induction of chromatid breaks with doses ≥ 0.02 Gy, but the frequency was not affected by KU55933 treatment in X-irradiated population with up to 0.08 Gy. This was in agreement with the result that 0.02-0.08 Gy of X-rays induce G2 arrest only a fraction of cells, if any (Figure 1). At higher doses the difference became more evident. With 0.4 Gy of X-rays, approximately one chromatid break per cell was observed in mitosis-progressing cells, whereas it was significantly increased by KU55933-treatment ($p < 0.01$). Average number of chromatid breaks per cell were 0.96 and 2.08 in the control and KU55933-treated population, respectively. As approximately 45% of metaphases showed chromatid breaks (Table 1), the number of chromatid breaks in cells with chromosome aberrations was estimated as around two. Thus, it was indicated that 4000~5000 SOID was equivalent to approximately two chromatid breaks, which correspond to a few DNA double strand breaks.

Discussion

Here we developed a novel parameter for quantifying DNA damage signal considering both the number and the size of the foci induced by IR. The new parameter, SOID, reflected an integrated amount of DNA damage signal in a single cell. We previously demonstrated that Ser15-phosphorylation level of p53 depends on focus size of Ser1981-phosphorylated ATM, and a single persistent phosphorylated ATM focus can deposit and emit DNA damage signal sufficient for G1 checkpoint induction through focus growth [30]. The finding indicates that not only the foci number, but also the foci size must be taken into consideration when DNA damage signal of foci is quantified. Indeed, we failed to observe

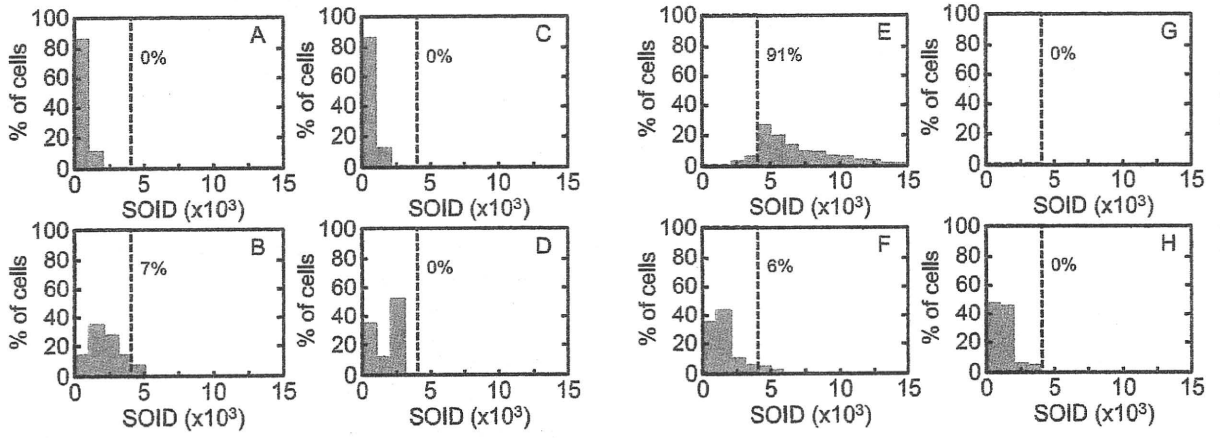

Figure 7 Distribution of the SOID values in G2 and mitotic cells. Exponentially-growing normal human primary fibroblasts were irradiated with 0.4 Gy of X-rays (A - D). Two hours after X-irradiation, cells were fixed and subjected to immunofluorescence staining for Ser139-phosphorylated H2AX and Ser10-phosphorylated H3. Cells were also exposed to 1.0 Gy of X-rays (E - H). They were fixed and subjected to immunofluorescence staining for Ser139-phosphorylated H2AX and Ser10-phosphorylated H3 at 2 hours (E and G), 6, 8 and 12 hours (F and H) later. The SOID values of phosphorylated H2AX foci in the control cells (A and C), 0.4 Gy-irradiated cells (B and D), and 1.0 Gy-irradiated cells (E - H) were measured. The SOID values obtained from 1.0 Gy-irradiated cells prepared at 6, 8 and 12 hours later were compiled in F and H. G2 cells (A, B, E and F) and mitotic cells (C, D, G and H) were identified as described in Figure 2. Dotted lines indicate 4000 SOID, and the numbers indicate the percentage of cells with the SOID above 4000.

significant difference in the number of phosphorylated H2AX foci between G2-arrested cells and mitosis-progressing cells after 0.4 Gy, while the dose induced apparent G2 arrest (Figure 3). In contrast, the SOID values visualized the difference between G2-arrested cells and mitosis-progressing cells. Thus, SOID could be a valuable parameter to qualify the amount of DNA damage signal required for G2/M checkpoint activation. As shown in Figure 4, it was quite evident that there was marked variations in the size and fluorescence intensity in each focus. Although the reason for the difference is currently unknown, one possible explanation could be that a focus with smaller size and weaker intensity may represents a residual signal of a DSB that is rejoined just before sample fixation. In any case, such possibility could also be the reason why the similar number of foci gives different SOID value between G2-arrested cells and mitosis-progressing cells. Thus, it can be concluded that the SOID is the better indicator for the quantity of DNA damage signals than the foci number alone.

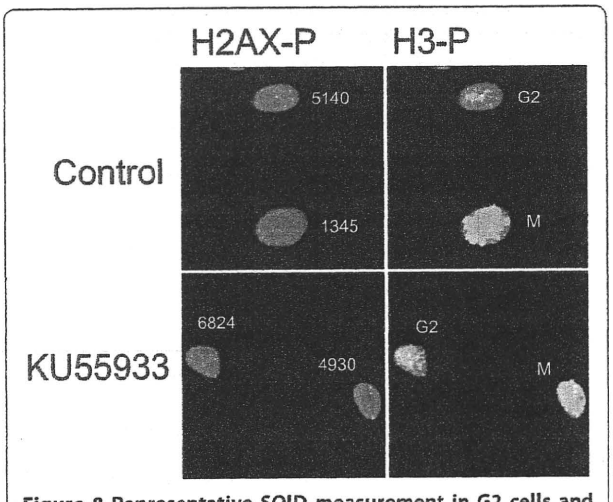

Figure 8 Representative SOID measurement in G2 cells and mitotic cells in the presence of KU55933. KU55933 (10 μM), or their solvent DMSO was treated from 30 min before IR. Two hours later, cells were fixed and subjected to immunofluorescence staining for Ser139-phosphorylated H2AX and Ser10-phosphorylated H3. KU55933 was washed out 30 minutes before fixation to recover the size and the fluorescence intensity of phosphorylated H2AX foci. Numbers indicate the SOID values in each nucleus.

A two-way comparison of the SOID between G2-arrested cells and mitosis-progressing cells, and between mitosis-progressing cells in the presence or absence of ATM or Chk1/2 inhibitor revealed that there was a threshold of SOID for G2 arrest, which is about 4000~5000. Our results demonstrated that most G2 cells with < 3000 SOID can evade G2/M checkpoint, however, there still be some few mitosis-progressing cells more than 3000 SOID. Therefore, it is more appropriate to conclude that the threshold of SOID for G2 arrest is about 4000~5000. Chromosome analysis revealed that such checkpoint-neglected cells progress to mitosis harbored ~2 chromatid breaks/cell. According to the previous estimation, in which one premature chromosome condensation (PCC) break is equated to

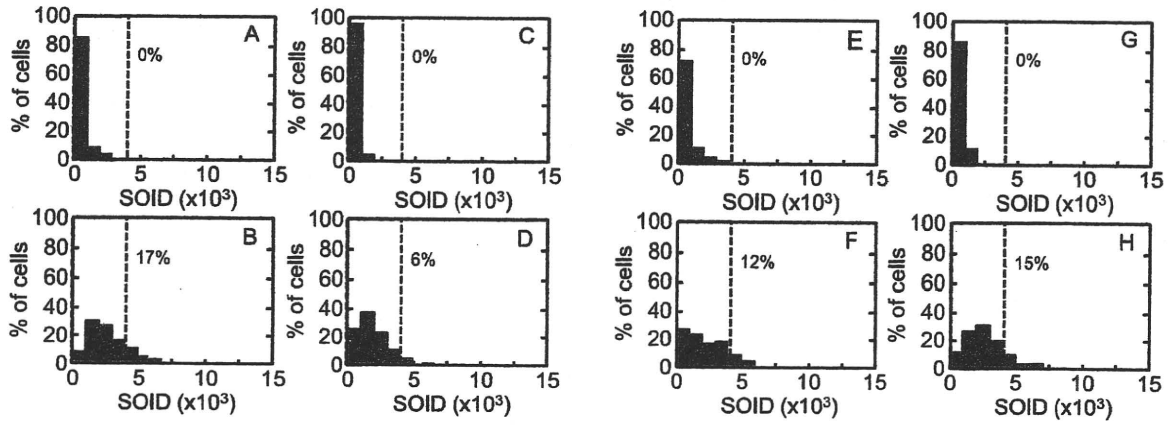

Figure 9 Distribution of the SOID values in G2 and mitotic cells treated with ATM or CHK1/2 inhibitor. Exponentially-growing normal human primary fibroblasts were irradiated with 0.4 Gy of X-rays in the presence of KU55933 (A - D) or SB218078 (E - H). Two hours later, cells were fixed and subjected to immunofluorescence staining for Ser139-phosphorylated H2AX and Ser10-phosphorylated H3. The SOID values of phosphorylated H2AX foci in the control cells (A, C, E and G) and 0.4 Gy-irradiated cells (B, D, F and H) were measured. G2 cells (A, B, E and F) and mitotic cells (C, D, G and H) were identified as described in Figure 2. Dotted lines indicate 4000 SOID, and the numbers indicate the percentage of cells with the SOID above 4000.

3~6 DSBs, 4000~5000 SOID could correspond to similar amount of DSBs [35]. In fact, foci number in Figure 3 was 7~9, which was comparable to the estimation. In contrast, inhibition of G2/M checkpoint by KU55933 or SB218078 allowed cells with ≥ 4000 SOID to enter mitosis (Figures 9). Inhibition of G2/M checkpoint by KU55933 also increased the number of chromatid breaks/cell, which was most pronounced after 0.4 Gy. These results indicate that the SOID value ≥ 4000 is biologically relevant. Cells with such amount of DNA damage signal of IR-induced foci elicit G2/M checkpoint, thereby minimizing the frequency of chromosome aberration in mitosis-progressing cells.

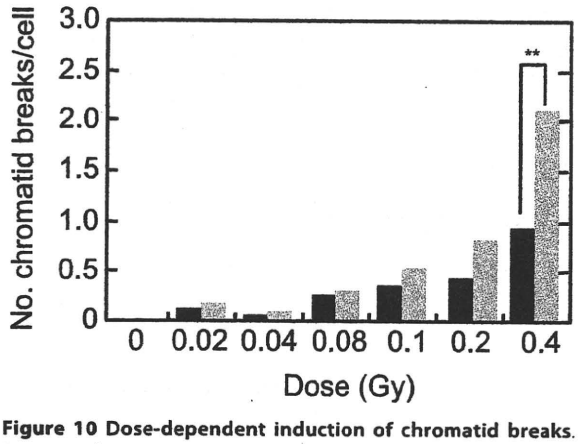

Figure 10 Dose-dependent induction of chromatid breaks. Exponentially-growing normal human primary fibroblasts were irradiated with 0, 0.02, 0.04, 0.08, 0.1, 0.2, and 0.4 Gy of X-rays, and two hours later, mitotic cells were harvested and chromosome samples were prepared. Colcemid (0.1 μg/ml) was treated from immediately after IR to 2 hr after IR in order to collect metaphase cells. KU55933 (10 μM) was treated from 30 min before IR to 1.5 hr after IR, and washed out, then media were replaced by fresh media containing DMSO and Colcemid. After the media replacement, cells were cultured for additional 30 min, followed by metaphase harvest. More than 50 metaphases were examined per point. Black bars: control cells, Grey bars: KU55933-treated cells. ** indicates significant difference at $p < 0.01$.

Previously, Deckbar et al. reported that G2/M checkpoint was imperfect, and its release occurred at a point when ~3.5 PCC breaks and 10~20 phosphorylated H2AX foci left. Based on the above estimation, they correspond to 10~20 DSBs remained [35]. We found that their threshold was clearly higher than that obtained in the present study. Although the reason for this discrepancy is not clear, a couple of points can be discussed. One of which is the size of the foci. We observed that there was an inverse relationship between the size and the number of foci. In fact, the size of the foci in cells with 10~20 foci was relatively small. Therefore, it seemed likely that the integrated DNA damage signal might be lower than the threshold, even the number of foci was 10~20. The second point could be the procedure used for counting the foci number. In the previous study, foci numbers in CENP-F-positive G2 cells exposed to 1 Gy of X-rays were counted. The number of the initial foci could be higher, and foci number was not determined in mitosis released from G2 arrest. In our examination, we counted foci numbers in phospho-H3-positive mitotic cells, predominantly in prophases. Therefore, we could determine the exact number of foci in cells passed through G2 arrest. Although these might or might not be the primary reason for the discrepancy, these observations again strengthened our claim that

Table 1 chromatid breaks induced by various doses of x-rays

Treatment	No. metaphases analyzed	No. metaphases with aberrations	No. of chromatid breaks
Control (+DMSO)			
0 Gy	55	1	1
0.02 Gy	59	7	8
0.04 Gy	61	3	3
0.08 Gy	75	11	16
0.1 Gy	70	15	21
0.2 Gy	50	14	18
0.4 Gy	55	25	53
+KU55933			
0 Gy	54	0	0
0.02 Gy	56	9	9
0.04 Gy	64	5	5
0.08 Gy	61	11	15
0.1 Gy	53	19	25
0.2 Gy	50	31	42
0.4 Gy	51	42	106

Cells were treated with KU55933 (10 μM) 30 minutes before irradiation until 30 minutes before metaphase harvest. Immediately after irradiation, colcemid (0.1 μM) was added to the medium, and cells were incubated for 2 hours. Then, metaphases were collected and chromosome samples were prepared as described in Methods.

not only the number but also the size of the foci must be considered in order to quantify the amount of DNA damage signal based on the foci.

Since the foci of phosphorylated histone H2AX were proved to be the most suitable and trustable surrogate marker for DSBs, several procedures have been developed to quantitate the amount of foci [14]. Once a reliable antibody against phophorylated H2AX foci was established, image-based assay was introduced to count the number of foci [36]. However, as described above, these assays were to count the number of foci and they were unable to measure the size of foci. Subsequently, flow-cytometry was introduced for automatic quantification of DNA damage signal based on total fluorescence obtained by immunofluorescnce assay [37,38], however, the assay could not account for the number of foci. Our current technique could unite these two procedures, which made the quantification of both the foci number and the size possible. The SOID value could be a novel parameter to evaluate DNA damage signal essential for genome integrity maintenance.

Conclusions

We developed a novel parameter for quantitative analysis of DNA damage signal, and we determined the threshold of DNA damage signal for IR-induced G2 arrest, which was represented by SOID 4000~5000. The present study emphasized that not only the foci number but also the size of the foci must be taken into consideration for the proper quantification of DNA damage signal.

Methods

Cell culture and irradiation

Low passage (4-9) normal human diploid primary fibroblasts were cultured in minimal essential Eagle's media (MEM) containing 10% fetal bovine serum (Thermo Fisher Scientific, USA) [30]. One to 4×10^4cells were seeded onto 22 x 22 mm coverslips in 35 mm dishes. Two days later, cells were irradiated with X-rays from X-ray generator (ISOVOLT TITAN 320, GE, USA) at 200 kV and 15 mA with a 0.5 mm copper filter at a dose rate of 0.2082 Gy/min. ATM inhibitor, KU55933 (Calbiochem, USA) was dissolved in DMSO to prepare 20 mM stock solution, and was treated at a final concentration of 10 μM. The KU55933 was treated from 30 min before X-ray-irradiation, and was washed out 30 min before fixation to recover size and fluorescence intensity of phosphorylated H2AX foci. Chk1/2 inhibitor, SB218078 (Calbiochem, USA) was dissolved in DMSO to prepare 2.5 mM stock solution, and was treated at a final concentration of 2.5 μM. The SB218078 was treated from 30 min before X-ray-irradiation to the time of fixation.

Immunofluorescence staining

Cells were once washed with 1 x PBS^-, and fixed with 4% formaldehyde in 1 x PBS^- for 10 min, then permeabilized with 0.5% Triton X-100 in 1 x PBS^- for 5 min. After permeabilization, the primary antibodies were applied for 2 hr in a 37°C humidified CO_2 incubator. After washing with 1 x PBS^-, the secondary antibodies conjugated with Alexa Fluor 488 or 594 (Invitrogen Life

Technologies Japan, Tokyo) were applied for 1 hr in the incubator. All antibodies were diluted in TBS-DT (20 mM Tris-HCl, pH7.6, 137 mM NaCl, 0.1% Tween 20, 125 μg/ml ampicillin, 5% skim milk). After washing with 1 x PBS$^-$, the coverslips were mounted onto slide glasses with 10% Glycerol in 1 x PBS$^-$. Nucleus was counterstained with DAPI. The primary antibodies used in this study were mouse anti-phosphorylated histone H2AX at serine 139 monoclonal antibody (clone 2F3, BioLegend, San Diego, CA), rabbit anti-phosphorylated histone H2AX at serine 139 polyclonal antibody (A300-081A, BETHYL, Montgomery, TX), mouse anti-phosphorylated histone H3 at serine 10 monoclonal antibody (Clone 3H10, Millipore Japan, Tokyo), rabbit anti-phosphorylated histone H3 at serine 10 polyclonal antibody (06-570, Millipore Japan, Tokyo).

Determination of Mitotic cells

Cells were incubated with anti-phosphorylated histone H3 at serine 10 followed by the incubation with the Alexa Fluor-labeled secondary antibody. The samples were scanned and imaged using IN Cell Analyzer 1000 (GE Healthcare Japan, Tokyo). Two-dimensional digital images were acquired using a 20X, 0.45NA objective lens and a 12-bit charged coupled device camera (GE Healthcare Japan, Tokyo). Images were processed and analyzed by IN Cell Investigator software (GE Healthcare Japan, Tokyo), and a fraction of cells with strong fluorescence signal was gated as mitotic cells. The original images corresponding to these cells were recalled and nuclear morphology was examined. Cells with condensed chromosomes were judged as mitotic cells. More than 5000 cells were analyzed per point.

Measurement of the SOID of phosphorylated-H2AX foci

The samples were scanned and imaged using IN Cell Analyzer 1000 (GE Healthcare Japan, Tokyo). Two-dimensional digital images were acquired using a 20X, 0.45NA objective lens and a 12-bit charged coupled device camera (GE Healthcare Japan, Tokyo). All images were captured with the same condition so that the background intensities were almost the same throughout the same series of experiments. Images were processed and analyzed by IN Cell Investigator software (GE Healthcare Japan, Tokyo). Nuclear area was determined by the DAPI fluorescence signal. Area (total pixel number) and mean fluorescence intensity per pixel of each phosphorylated-H2AX focus, and the number of foci per cell were obtained by IN Cell Investigator software using the original parameters provided by IN Cell Developer software (GE Healthcare Japan, Tokyo). Then, the SOID was calculated by IN Cell Investigator.

The SOID was defined as the sum of fluorescence of each focus within one nucleus. The SOID was calculated for individual nucleus as the sum of (area (total pixel numbers) of each focus) x (mean fluorescence intensity per pixel of each focus). We set background threshold of foci so that the foci number scored by IN Cell Analyzer is identical to that scored by eye. To compare the SOID values between G2 and mitotic cells, G2 cells were discriminated from mitotic cells based upon nuclear morphology and phosphorylated histone H3 signal. G2 cells had weaker intensity and more rugged and discontinuous pattern of phosphorylated histone H3 signal compared to mitotic cells. Mitotic cells showed condensed chromosomes, which became visible in prophase. As phosphorylated histone H2AX foci in metaphases and anaphases were not suitable for proper quantitative analysis, the SOID value in mitotic cells was calculated predominantly in prophases. Approximately 5000 cells from multiple coverslips were scanned.

Preparation of chromosome samples and chromosome analysis

Exponentially-growing normal human primary fibroblasts were treated with 10 μM KU55933, or its solvent DMSO 30 min before irradiation. Then, cells were irradiated with 0.02, 0.04, 0.08, 0.1, 0.2, and 0.4 Gy of X-rays. Immediately after irradiation, Colcemid (Invitrogen Life Technologies Japan, Tokyo) was added at a final concentration of 0.1 μg/ml to collect metaphase cells. Two hours later, metaphases were harvested by brief trypsinization and tapping flasks. KU55933 was washed out 30 min before metaphase harvest to make experimental condition identical to the SOID experiment. Harvested cells were once washed with 1 x PBS$^-$, and then, 0.075 M KCl was treated for 20 min at ambient temperature to swell cells. After the hypotonic treatment, cells were fixed with Carnoy's fixative (methanol : acetic acid = 3 : 1) for 30 min on ice. Then, cells were resuspended with appropriate volume of Carnoy's fixative, and dropped onto 70% ethanol-immersed slide glasses. After drying overnight, slide glasses were stained with 6.5% Giemsa staining solution. Chromatid breaks were scored by eye, and at least 50 metaphases were analyzed per point.

Data analysis

Wilcoxon rank test was used to evaluate significant difference between two groups. P values of less than 0.05 were considered significant difference.

Acknowledgements

This work was supported by Global COE program in Nagasaki University, and Grant-in-Aid for Scientific Research from Japan Society for the Promotion of Science.

Authors' contributions

AI conceived of the study, carried out the immunoflorescence study, and drafted the manuscript. MY carried out the immunoflorescence study,

performed the statistical analysis, and drafted the manuscript. KS participated in the design of the study. SY helped to draft the manuscript. All authors read and approved the final manuscript.

Competing interests
The authors declare that they have no competing interests.

Received: 9 May 2010 Accepted: 4 August 2010
Published: 4 August 2010

References

1. Hartwell LH, Weinert TA: **Checkpoints: controls that ensure the order of cell cycle events.** *Science* 1989, **246**:629-634.
2. Elledge SJ: **Cell cycle checkpoints: preventing an identity crisis.** *Science* 1996, **274**:1664-1672.
3. Savitsky K, Bar-Shira A, Gilad S, Rotman G, Ziv Y, Vanagaite L, Tagle DA, Smith S, Uziel T, Sfez S, Ashkenazi M, Pecker I, Frydman M, Harnik R, Patanjali SR, Simmons A, Clines GA, Sartiel A, Gatti RA, Chessa L, Sanal O, Lavin MF, Jaspers NG, Taylor AM, Arlett CF, Miki T, Weissman SM, Lovett M, Collins FS, Shiloh Y: **A single ataxia telangiectasia gene with a product similar to PI-3 kinase.** *Science* 1995, **268**:1749-1753.
4. Bakkenist CJ, Kastan MB: **DNA damage activates ATM through intermolecular autophosphorylation and dimer dissociation.** *Nature* 2003, **421**:499-506.
5. Matsuoka S, Ballif BA, Smogorzewska A, McDonald ER, Hurov KE, Luo J, Bakalarski CE, Zhao Z, Solimini N, Lerenthal Y, Shiloh Y, Gygi SP, Elledge SJ: **ATM and ATR substrate analysis reveals extensive protein networks responsive to DNA damage.** *Science* 2007, **316**:1160-1166.
6. Melchionna R, Chen XB, Blasina A, McGowan CH: **Threonine 68 is required for radiation-induced phosphorylation and activation of Cds1.** *Nat Cell Biol* 2000, **2**:762-765.
7. Ahn JY, Schwarz JK, Piwnica-Worms H, Canman CE: **Threonine 68 phosphorylation by ataxia telangiectasia mutated is required for efficient activation of Chk2 in response to ionizing radiation.** *Cancer Res* 2000, **60**:5934-5936.
8. Iliakis G, Wang Y, Guan J, Wang H: **DNA damage checkpoint control in cells exposed to ionizing radiation.** *Oncogene* 2003, **22**:5834-5847.
9. Rogakou EP, Pilch DR, Orr AH, Ivanova VS, Bonner WM: **DNA double-stranded breaks induce histone H2AX phosphorylation on serine 139.** *J Biol Chem* 1998, **273**:5858-5868.
10. Burma S, Chen BP, Murphy M, Kurimasa A, Chen DJ: **ATM phosphorylates histone H2AX in response to DNA double-strand breaks.** *J Biol Chem* 2001, **276**:42462-42467.
11. Friesner JD, Liu B, Culligan K, Britt AB: **Ionizing radiation-dependent gamma-H2AX focus formation requires ataxia telangiectasia mutated and ataxia telangiectasia mutated and Rad3-related.** *Mol Cell Biol* 2005, **16**:2566-2576.
12. Stiff T, O'Driscoll M, Rief N, Iwabuchi K, Löbrich M, Jeggo PA: **ATM and DNA-PK function redundantly to phosphorylate H2AX after exposure to ionizing radiation.** *Cancer Res* 2004, **64**:2390-2396.
13. Rogakou EP, Boon C, Redon C, Bonner WM: **Megabase chromatin domains involved in DNA double-strand breaks in vivo.** *J Cell Biol* 1999, **146**:905-916.
14. Löbrich M, Shibata A, Beucher A, Fisher A, Ensminger M, Goodarzi AA, Barton O, Jeggo PA: **GammaH2AX foci analysis for monitoring DNA double-strand break repair: strengths, limitations and optimization.** *Cell cycle* 2010, **9**:662-669.
15. Goldberg M, Stucki M, Falck J, D'Amours D, Rahman D, Pappin D, Bartek J, Jackson SP: **MDC1 is required for the intra-S-phase DNA damage checkpoint.** *Nature* 2003, **421**:952-956.
16. Lou Z, Minter-Dykhouse K, Wu X, Chen J: **MDC1 is coupled to activated CHK2 in mammalian DNA damage response pathways.** *Nature* 2003, **421**:957-961.
17. Stewart GS, Wang B, Bignell CR, Taylor AM, Elledge SJ: **MDC1 is a mediator of the mammalian DNA damage checkpoint.** *Nature* 2003, **421**:961-966.
18. Schultz LB, Chehab NH, Malikzay A, Halazonetis TD: **p53 binding protein 1 (53BP1) is an early participant in the cellular response to DNA double-strand breaks.** *J Cell Biol* 2000, **151**:1381-1390.
19. Mailand N, Bekker-Jensen S, Faustrup H, Melander F, Bartek J, Lukas C, Lukas J: **RNF8 ubiquitylates histones at DNA double-strand breaks and promotes assembly of repair proteins.** *Cell* 2007, **131**:887-900.
20. Huen MS, Grant R, Manke I, Minn K, Yu X, Yaffe MB, Chen J: **RNF8 transduces the DNA-damage signal via histone ubiquitylation and checkpoint protein assembly.** *Cell* 2007, **131**:901-914.
21. Kolas NK, Chapman JR, Nakada S, Ylanko J, Chahwan R, Sweeney FD, Panier S, Mendez M, Wildenhain J, Thomson TM, Pelletier L, Jackson SP, Durocher D: **Orchestration of the DNA-damage response by the RNF8 ubiquitin ligase.** *Science* 2007, **318**:1637-1640.
22. Wang B, Elledge SJ: **Ubc13/Rnf8 ubiquitin ligases control foci formation of the Rap80/Abraxas/Brca1/Brcc36 complex in response to DNA damage.** *Proc Natl Acad Sci USA* 2007, **104**:20759-20763.
23. Maser RS, Monsen KJ, Nelms BE, Petrini JH: **hMre11 and hRad50 nuclear foci are induced during the normal cellular response to DNA double-strand breaks.** *Mol Cell Biol* 1997, **17**:6087-6096.
24. Ito A, Tauchi H, Kobayashi J, Morishima K, Nakamura A, Hirokawa Y, Matsuura S, Ito K, Komatsu K: **Expression of full-length NBS1 protein restores normal radiation responses in cells from Nijmegen breakage syndrome patients.** *Biochem Biophys Res Commun* 1999, **265**:716-721.
25. Lou Z, Minter-Dykhouse K, Franco S, Gostissa M, Rivera MA, Celeste A, Manis JP, van Deursen J, Nussenzweig A, Paull TT, Alt FW, Chen J: **MDC1 maintains genomic stability by participating in the amplification of ATM-dependent DNA damage signals.** *Mol Cell* 2006, **21**:187-200.
26. Wilson KA, Stern DF: **NFBD1/MDC1, 53BP1 and BRCA1 have both redundant and unique roles in the ATM pathway.** *Cell Cycle* 2008, **7**:3584-3594.
27. Falck J, Coates J, Jackson SP: **Conserved modes of recruitment of ATM, ATR and DNA-PKcs to sites of DNA damage.** *Nature* 2005, **434**:605-611.
28. Fernandez-Capetillo O, Chen HT, Celeste A, Ward I, Romanienko PJ, Morales JC, Naka K, Xia Z, Camerini-Otero RD, Motoyama N, Carpenter PB, Bonner WM, Chen J, Nussenzweig A: **DNA damage-induced G2-M checkpoint activation by histone H2AX and 53BP1.** *Nat Cell Biol* 2002, **4**:993-997.
29. Wang B, Matsuoka S, Carpenter PB, Elledge SJ: **53BP1, a mediator of the DNA damage checkpoint.** *Science* 2002, **298**:1435-1438.
30. Yamauchi M, Oka Y, Yamamoto M, Niimura K, Uchida M, Kodama S, Watanabe M, Sekine I, Yamashita S, Suzuki K: **Growth of persistent foci of DNA damage checkpoint factors is essential for amplification of G1 checkpoint signaling.** *DNA repair* 2008, **7**:405-417.
31. Suzuki M, Suzuki K, Kodama S, Watanabe M: **Phosphorylated histone H2AX foci persist on rejoined mitotic chromosomes in normal human diploid cells exposed to ionizing radiation.** *Radiat Res* 2006, **165**:269-276.
32. Nelson G, Buhmann M, von Zglinicki T: **DNA damage foci in mitosis are devoid of 53BP1.** *Cell Cycle* 2009, **8**:3379-3383.
33. Hickson I, Zhao Y, Richardson CJ, Green SJ, Martin NM, Orr AI, Reaper PM, Jackson SP, Curtin NJ, Smith GC: **Identification and characterization of a novel and specific inhibitor of the ataxia-telangiectasia mutated kinase ATM.** *Cancer Res* 2004, **64**:9152-9159.
34. Jackson JR, Gilmartin A, Imburgia C, Winkler JD, Marshall LA, Roshak A: **An indolocarbazole inhibitor of human checkpoint kinase (Chk1) abrogates cell cycle arrest caused by DNA damage.** *Cancer Res* 2000, **60**:566-572.
35. Deckbar D, Birraux J, Krempler A, Tchouandong L, Beucher A, Walker S, Stiff T, Jeggo P, Löbrich M: **Chromosome breakage after G2 checkpoint release.** *J Cell Biol* 2007, **176**:749-755.
36. Rothkamm K, Lobrich M: **Evidence for a lack of DNA double-strand break repair in human cells exposed to very low x-ray doses.** *Proc Natl Acad Sci USA* 2003, **100**:5057-5062.
37. Olive PL: **Detection of DNA damage in individual cells by analysis of histone H2AX phosphorylation.** *Methods Cell Biol* 2004, **75**:355-373.
38. Tanaka T, Halicka D, Traganos F, Darzynkiewicz Z: **Cytometric analysis of DNA damage: phosphorylation of histone H2AX as a marker of DNA double-strand breaks (DSBs).** *Methods Mol Biol* 2009, **523**:161-168.

doi:10.1186/2041-9414-1-10
Cite this article as: Ishikawa *et al.*: **Image-based quantitative determination of DNA damage signal reveals a threshold for G2 checkpoint activation in response to ionizing radiation.** *Genome Integrity* 2010 **1**:10.

Suzuki *et al. Genome Integrity* 2010, **1**:4
http://www.genomeintegrity.com/content/1/1/4

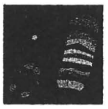

GENOME INTEGRITY

RESEARCH Open Access

Requirement of ATM-dependent pathway for the repair of a subset of DNA double strand breaks created by restriction endonucleases

Keiji Suzuki*†, Maiko Takahashi*†, Yasuyoshi Oka, Motohiro Yamauchi, Masatoshi Suzuki and Shunichi Yamashita

Abstract

Background: DNA double strand breaks induced by DNA damaging agents, such ionizing radiation, are repaired by multiple DNA repair pathways including non-homologous end-joining (NHEJ) repair and homologous recombination (HR) repair. ATM-dependent DNA damage checkpoint regulates a part of DNA repair pathways, however, the exact role of ATM activity remains to be elucidated. In order to define the molecular structure of DNA double strand breaks requiring ATM activity we examined repair of DNA double strand breaks induced by different restriction endonucleases in normal human diploid cells treated with or without ATM-specific inhibitor.

Results: Synchronized G1 cells were treated with various restriction endonucleases. DNA double strand breaks were detected by the foci of phosphorylated ATM at serine 1981 and 53BP1. DNA damage was detectable 2 hours after the treatment, and the number of foci decreased thereafter. Repair of the 3'-protruding ends created by *Pst* I and *Sph* I was efficient irrespective of ATM function, whereas the repair of a part of the blunt ends caused by *Pvu* II and *Rsa* I, and 5'-protruding ends created by *Eco* RI and *Bam* HI, respectively, were compromised by ATM inhibition.

Conclusions: Our results indicate that ATM-dependent pathway plays a pivotal role in the repair of a subset of DNA double strand breaks with specific end structures.

Background

Ionizing radiation induces various types of DNA damage, among which DNA double strand breaks show the most detrimental effects on living cells. DNA double strand breaks are repaired by two major DNA repair pathways, which are non-homologous end-joining (NHEJ) and homologous recombination (HR) [1-6]. While DNA repair pathway efficiently rejoin the broken ends, unrejoined or mis-rejoined DNA damage provide chances to threaten the integrity of the genome [7-9]. Thus, the cells evolved a sophisticated system, by which stability of the genome is maintained [10,11]. The system referred to as DNA damage checkpoint pathway requires ATM function [12-14], which is activated by dissociation of ATM proteins followed by autophosphorylation [15]. Activated ATM phosphorylates various downstream proteins including those that regulate cell cycle progression, cell death, as well as DNA repair [11,14,16,17]. Thereby, ATM plays a critical role in orchestrating DNA damage signaling and DNA damage repair.

Although AT cells were known to be sensitive to ionizing radiation, the mechanism underlying the hyper radiosensitivity has not yet been fully understood [12-14,18]. AT cells have no gross defect in DNA double strand break repair, however, several studies reported that a fraction of the initial DNA double strand breaks remained unrejoined in AT cells [19-23]. While most of the DNA double strand breaks are repaired by DNA-PK-dependent nonhomologous end-joining (NHEJ), a subset of breaks, which are refractory to DNA repair, might require Artemis for processing [6,23,24]. As Artemis activity is regulated by phosphorylation by ATM [23,25-27], it was suggested that a lack of Artemis activity explains increased radiosensitivity of AT cells.

More recently, another possibility was proposed, in which ATM activity is required for reorganization of heterochromatin through phosphorylation of Kruppel-asso-

* Correspondence: kzsuzuki@nagasaki-u.ac.jp, dm07134c@cc.nagasaki-u.ac.jp
Atomic Bomb Disease Institute, Nagasaki University Graduate School of Biomedical Sciences, 1-12-4 Sakamoto, Nagasaki 852-8523, Japan
† Contributed equally
Full list of author information is available at the end of the article

ciated box-associated protein-1 (KAP1) [28]. This idea was based on the understanding that DNA damage foci in heterochromatin regions are more refractory to repair than those in euchromatin regions [29-32]. Mobilization of KAP-1 by ATM-dependent phosphorylation is necessary for foci removal from heterochromatin [33], suggesting that cells lacking ATM function accumulate residual DNA double strand breaks in heterochromatin regions. However, there was no direct evidence showing actual DNA double strand breaks persisted in heterochromatin. It was also reported that other ATM-independent mechanisms were involved in DNA repair in heterochromatin. For example, ATM-independent mobilization of HP1 from chromatin increased accessibility of DNA double strand breaks by repair factors [34]. Local chromatin relaxation in the vicinity of DNA double strand breaks was also mediated by ATP-dependent mechanism [29]. Thus, multiple pathways are involved in heterochromatic DNA repair. Therefore, it is still possible that increased radiosensitivity of AT cells does not solely stem from inability to repair DNA double strand breaks in heterochromatin [35].

Recently, cell cycle-dependent repair of DNA double strand breaks was examined in AT and Artemis-defective cells [22]. Since residual fractions of foci were similar between AT and Artemis-defective cells in G1, a subset of DNA double strand breaks seems to require processing by Artemis-dependent pathway. Therefore, we have asked whether any specific types of broken ends require ATM-dependent repair pathway. Here, we examined the repair kinetics of DNA double strand breaks in synchronized G1 cells treated with different restriction enzymes. Restriction endonucleases were introduced into cells by electroporation [36]. We found that ATM inhibition by KU55933 partially compromised repair of DNA double strand breaks created by *Pvu* II, *Rsa* I, *Eco* RI, and *Bam* HI, but not by *Pst* I and *Sph* I, indicating that ATM-dependent pathway is required for processing certain types of termini. Our results propose that a part of radiosensitivity in AT cells could be explained by defective repair of certain types of DNA double strand breaks induced by ionizing radiation.

Results

Induction of DNA damage foci by restriction endonuclease treatments

Induction of DNA double strand breaks was examined by the foci formation of phosphorylated ATM and 53BP1. Because cells were electroporated in the presence of enzyme reaction buffer, we checked whether these conditions affected foci formation or not. As shown in Figure 1, electroporation of *Pvu* II induced phosphorylated ATM foci and 53BP1 foci, whereas no focus induction was observed in cells that underwent electroporation with

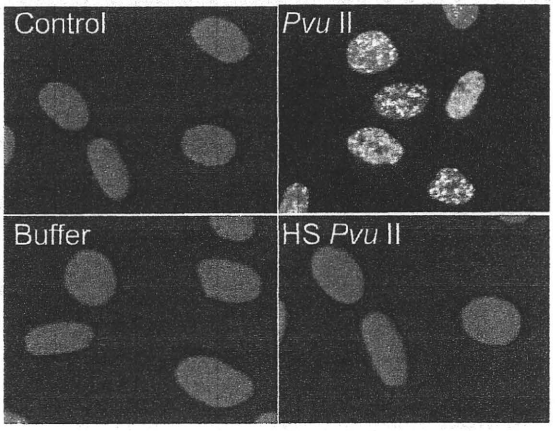

Figure 1 Electroporation of cells with restriction endonucleases. Synchronized normal human diploid cells in G1 were collected by trypsinization and suspended in PBS buffer. Enzyme reaction buffer and *Pvu* II (100 U) were mixed immediately before electroporation as described in METHODS. Cells were incubated for 2 hours before fixation. Control; no treatment, Buffer; cells were electroporated with reaction buffer, *Pvu* II; cells were treated with 100 U of *Pvu* II, HS *Pvu* II, cells were electroporated with *Pvu* II (100 U) heat inactivated at 80°C for 20 minutes.

buffer only. We also confirmed that the foci formation was dependent upon the enzyme activity, since cells electroporated with heat-inactivated *Pvu* II did not induce foci (HS *Pvu* II).

A variety of endonucleases were used in this study. Group I restriction endonucleases include *Pvu* II, *Rsa* I, *Bgl* I, *Eco* RV and *Sma* I, which create blunt ends. Group II enzymes including *Pst* I, *Sph* I, and *Kpn* I generate 3'-protruding ends. Group III enzymes include *Eco* RI, *Bam* HI, *Not* I, *Hind* III, and *Hinf* I, which produce 5'-protruding ends. While dose-dependent increase of foci-positive cells was observed, we decided to use 100 units as they were the optimum condition for the detection of the foci. Electroporation of cells with *Pvu* II, *Rsa* I, *Pst* I, *Sph* I and *Eco* RI induced foci in more than 80% of cells, while *Eco* RV, *Bam* HI and *Hinf* I could induce foci in approximately 50% of cells. In contrast, little or no foci was induced by 100 units of *Bgl* I, *Sma* I, *Kpn* I, *Not* I and *Hind* III, and no effect was observed even with increasing the amount of enzymes. Therefore, in the following experiments, we used six restriction endonucleases including *Pvu* II, *Rsa* I, *Pst* I, *Sph* I, *Eco* RI and *Bam* HI.

After electroporation with restriction endonucleases, cells were incubated for 2 hours, which allow cells to attach on the coverslips. At this point, more than 90% of cells showed the signal of ATM phosphorylation (Figure 2). As shown in Figure 3, 30~40% of cells showed diffused foci signal throughout the nuclei, which were classified as Type I nuclei (Figure 3). Approximately 30% of cells had numerous foci, whose number was more than 30 (Type II

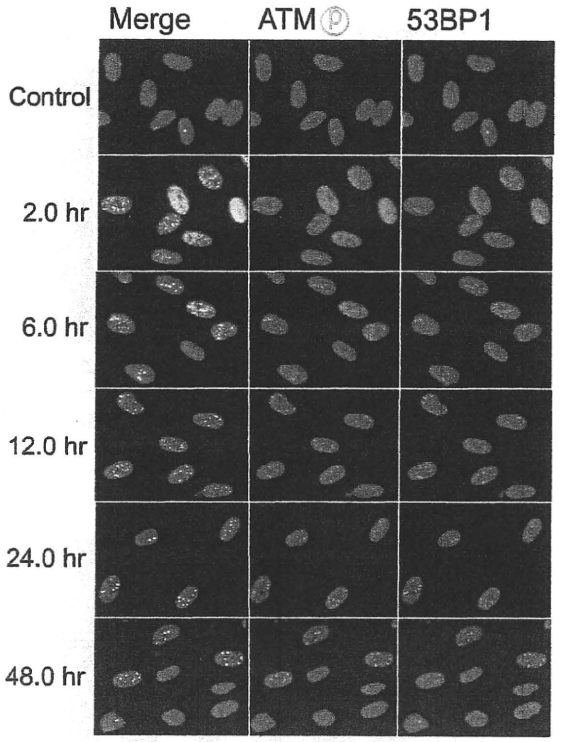

Figure 2 Time-dependent foci formation by Pvu II. Synchronized normal human diploid cells in G1 were electroporated with *Pvu* II (100 U) as described in METHODS. The cells were incubated for the time indicated before fixation.

nuclei), while 10~20% of cells contained countable numbers of foci (1~30)(Type III nuclei). Type IV nuclei were those without any foci. It should be noted that 53BP1 foci could not be detected in Type I nuclei. This is because 53BP1 is the protein recruited to the sites of phosphorylated ATM foci. Therefore, if multiple tiny foci of phosphorylated ATM were evenly distributed within the nucleus, 53BP1 might not be detected as the foci. In Type II and III nuclei, 53BP1 foci were always colocalized with phosphorylated ATM foci. Activated ATM transduces DNA damage signal through phosphorylation of the downstream effectors. In fact, we confirmed that phosphorylated ATM foci were also colocalized with phosphorylated 53BP1, phosphorylated histone H2AX, and phosphorylated NBS1 (See Additional file 1). In the subsequent study, we counted the number of 53BP1 foci colocalized with phosphorylated ATM foci.

Repair of restriction endonuclease-induced foci

Time-dependent decrease in the foci number was examined (Figure 2). After electroporation, at least one hour was needed to allow cells for firm attachment. Two hours after the treatment, the foci were already induced maximally, and more than 90% of cells were foci-positive after *Pvu* II-treatment (Figure 4). The percentage of Type I nuclei gradually disappeared thereafter, and more than 50% of cells lost foci within 24 hours after the treatment. By 48 hours after the treatment, more than 80% of cells repaired foci. Because the number of foci per nucleus was not uniformly distributed, the number of foci-negative cells might be overestimated by growth of the cells that were released from cell cycle arrest. Therefore, repair of foci was also assessed by the distribution of foci number per nucleus. As shown in Figure 3, the number of foci was also decreased with increasing times after the treatment. Between 6 and 24 hours after the treatment, the fraction of Type III nuclei seemed to be unchanged, as Type I and II nuclei were shifted to Type III nuclei, but the number of foci apparently decreased, indicating repair of DNA damage foci in Type III nuclei. Similar results were

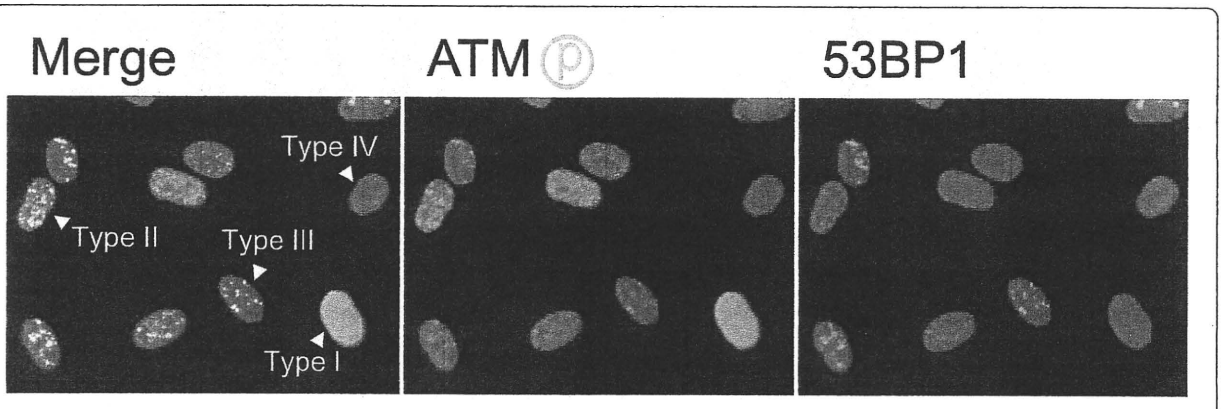

Figure 3 Classification of the nuclei with foci. Synchronized normal human diploid cells in G1 were electroporated with *Pvu* II (100 U) as described in METHODS, and they were incubated for 2 hours before fixation. The nuclei were classified into 4 types. Type I; nuclei with diffused phosphorylated ATM signal, but without 53 BP1 foci. Type II; nuclei with numerous foci more than 30 foci. Type III; nuclei with countable foci below 30. Type IV; nuclei without detectable foci.

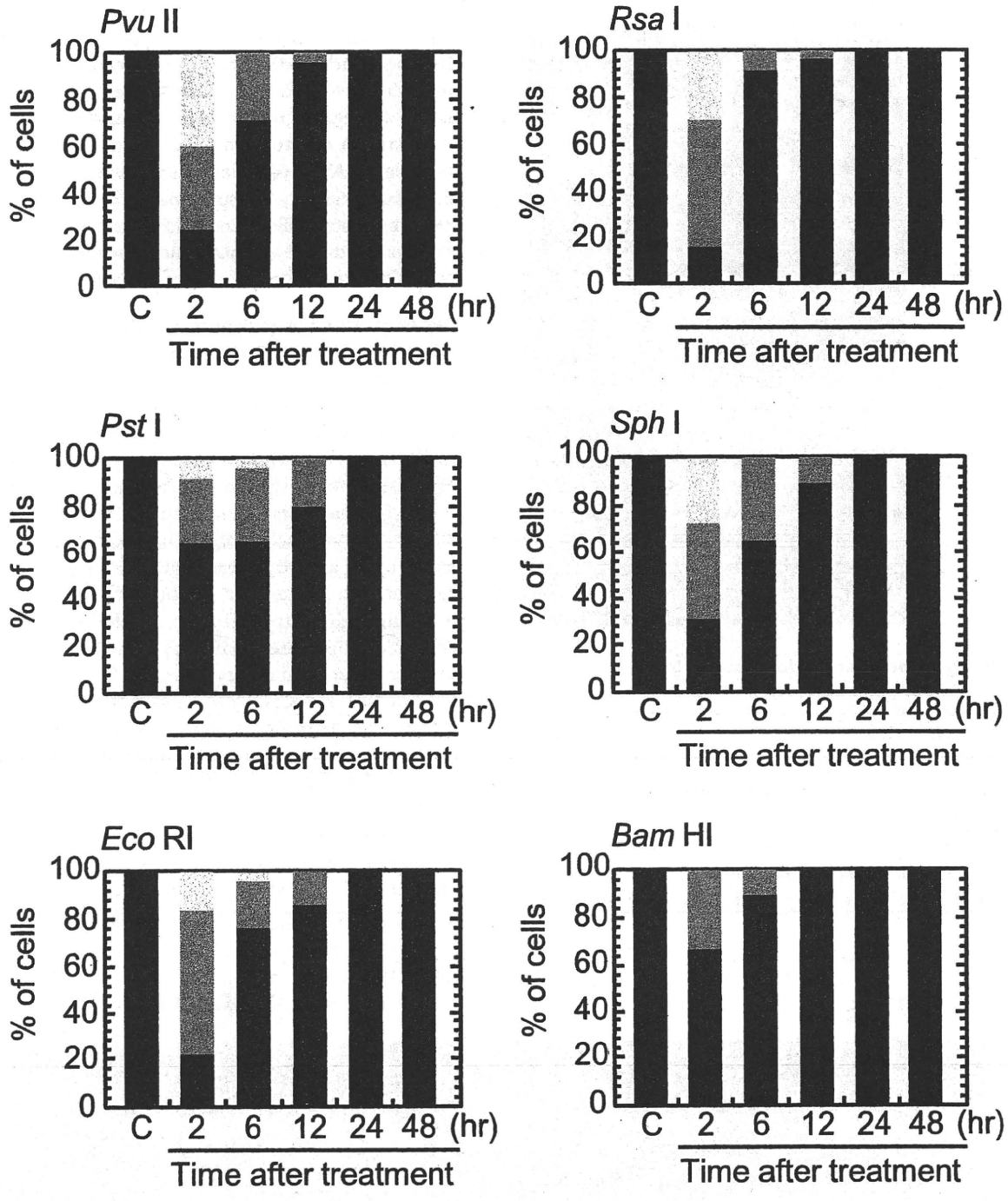

Figure 4 Distribution of cells with different nuclear type. Synchronized normal human diploid cells in G1 were electroporated with 100 U of various restriction endonucleases as described in METHODS. The cells were incubated for the time indicated before fixation. At least 1000 nuclei were examined. C; mock-treated control cells without restriction endonucleases. Black bars represent cells without foci (Type IV). Dark gray and light gray bars represent cells with Type III and Type II nuclei, respectively. Off-white bars represent cells with Type I nuclei.

obtained in every cell treated with *Rsa* I, *Pst* I, *Sph* I, *Eco* RI and *Bam* HI (Figure 4).

Effects of ATM inactivation on DNA damage foci repair

Role of ATM-dependent repair pathway were examined by inhibiting ATM activity using an ATM specific inhibitor, KU55933. Suppression of ATM activity was checked by significant loss of phosphorylation of ATM at serine 1981 (Figure 5). Accordingly, foci formation of 53 BP1 was significantly compromised, although the effect was less profound compared with the suppressive effect on phosphorylated ATM foci. Because inhibition of ATM activity by KU55933 is reversible, the formation of phosphorylated ATM foci and 53 BP1 foci was visualized by incubating cells for 0.5 hour with a fresh medium without KU55933. The percentage of cells with Type III and IV nuclei was compared 24, 36, and 48 hours after the treatment. We confirmed that KU55933 treatment alone did not show any effect on the foci type distribution in the control cells. As shown in Figure 6, the increase of foci-negative nuclei was suppressed by KU55933 in cells treated with *Pvu* II, *Rsa* I, *Eco* RI and *Bam* HI, whereas, no such effect was observed in *Pst* I and *Sph* I-treated cells. The effect of KU55933 was more pronounced when the number of foci in Type III nuclei was compared (Figure 7). The distribution of foci number clearly showed an inhibitory effect of DNA damage foci repair by ATM inhibition in *Pvu* II, *Rsa* I, *Eco* RI, and *Bam* HI-treated cells (Figures 8 and 9). In contrast, the distribution of foci number does not show any significant difference in cells treated with *Pst* I and *Sph* I (Figure 10).

Discussion

Use of restriction endonucleases to study the biological effects of DNA double strand breaks has been described for many years [36-38]. Previously, the formation of DNA double strand breaks was quantified by chromosome aberrations or by comet assay in restriction endonuclease-treated Chinese hamster cells [39-41] and human lymphoblastoid cells [37,38,40]. Here, we introduced various restriction endonucleases into G1-synchronized normal human fibroblast-like cells, and DNA double strand breaks were successfully detected by phosphorylated ATM foci and 53 BP1 foci. It is well established that the foci of DNA damage checkpoint factors can be used as reliable markers for DNA double strand breaks [42-44]. As phosphorylation of such factors was also induced in response to various stresses [45-47], we carefully determined whether electroporation by itself or the introduction of exogenous proteins did not cause phosphorylation of ATM. As shown in Figure 1, neither treatment with reaction buffer only nor electroporation with heat-inactivated *Pvu* II induced foci, indicating that foci formation exclusively depended upon the enzyme activity. Although various types of restriction endnucleases were examined in this study, not all of them were functional in normal human cells. The reason of this result was not known, but biochemical conditions including salt concentration might not be appropriate in the intact nuclei for some enzymes. According to the result shown in Figure 2, at least two-hour incubation after electroporation was sufficient for inducing DNA double strand breaks. Since the fraction of foci-negative cells was already increased slightly six hours after *Pvu* II treatment (Figure 4), the enzyme activity seemed to be active for the first few hours. Repair of DNA double strand breaks induced by restriction endonucleases was confirmed by the increase of the fraction of cells without foci (Type IV nuclei). It was also evidenced when the distribution of foci numbers in Type III nuclei was compared (Figures 8, 9 and 10).

Involvement of ATM-dependent pathway in foci repair was examined by inhibiting ATM activity by KU55933, which is a specific inhibitor for ATM [48]. As shown in Figures 5 and 7, KU55933 treatment significantly compromised phosphorylation of ATM, indicating that ATM activity was considerably inhibited. While the suppressive effect was less significant in 53 BP1 foci, it could be explained by phosphorylation-independent accumulation of 53 BP1, as described previously [49]. The increase in the fraction of Type IV nuclei was delayed by KU55933 in cells treated with *Pvu* II, *Rsa* I, *Eco* RI, and *Bam* HI. Although such inhibitory effects were not apparent at early times after the treatment (data not shown), noticeable effect was observed at later times (Figure 6). Similar result was reported in AT cells exposed to X-rays, in which no repair defect during 2 hours incubation after X-irradiation but the fraction of residual damage was significantly higher [22]. More striking effects were observed when the distribution of foci number was compared (Figures 8 and 9). Importantly, these inhibitory effects were not entirely detected in cells treated with *Pst* I and *Sph* I

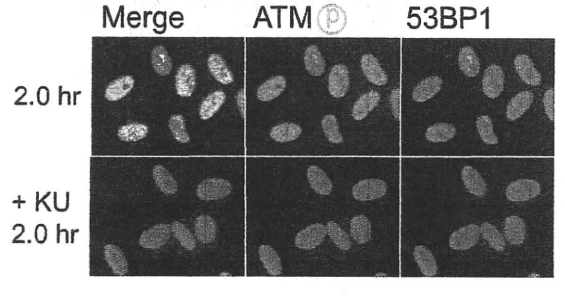

Figure 5 Effect of ATM inhibitor on foci formation. Synchronized normal human diploid cells in G1 were electroporated with *Pvu* II (100 U) as described in METHODS, and they were incubated for 2 hours before fixation. KU55933 (20 μM) was administrated 30 minutes before electroporation, and the cells were incubated with a medium containing KU55933 after electroporation.

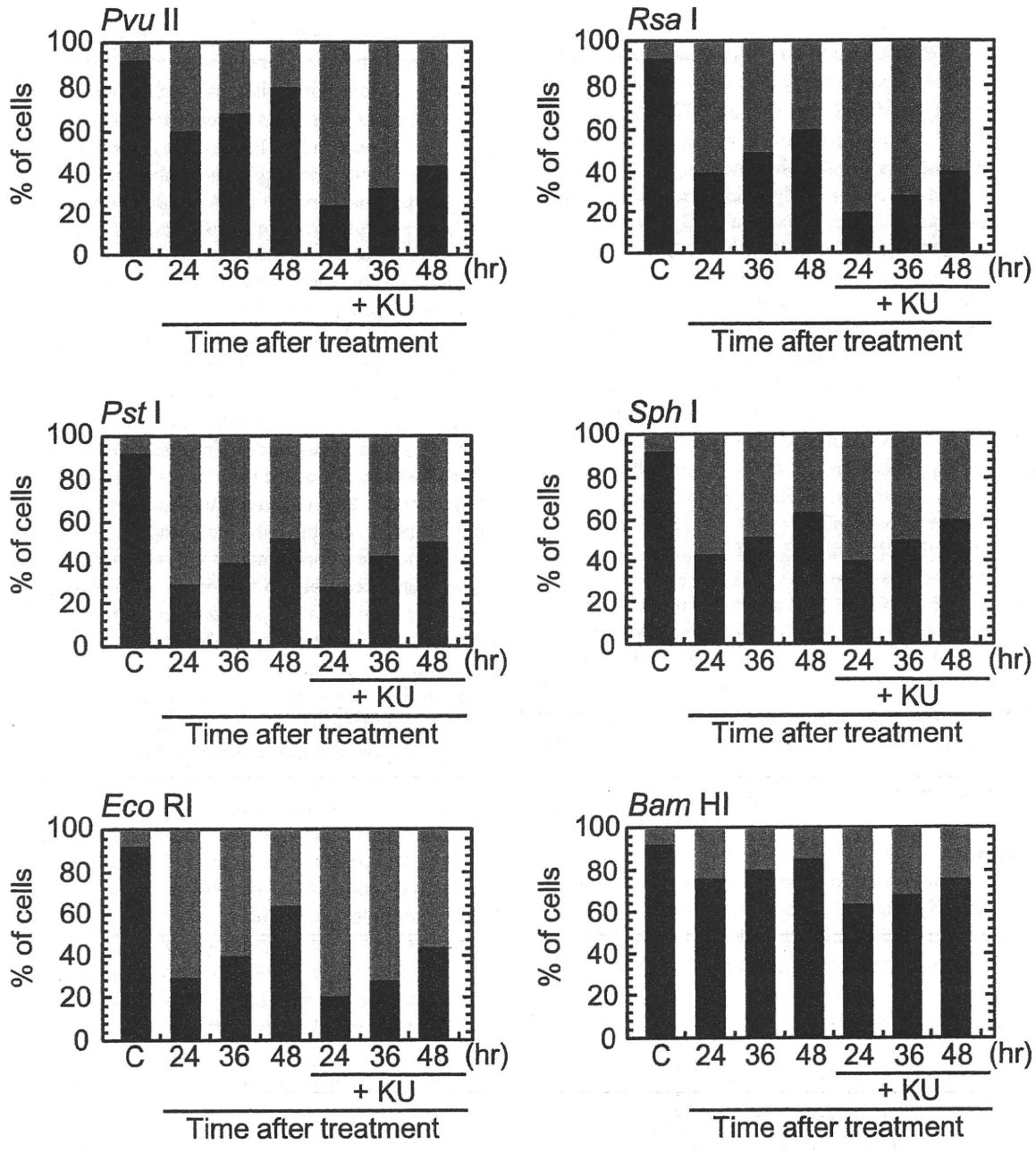

Figure 6 Effect of ATM inhibition on DNA damage foci repair Synchronized normal human diploid cells in G1 were electroporated with 100 U of various restriction endonucleases with or without 20 μM KU55933. The cells were incubated for the time indicated before fixation. At least 1000 nuclei were examined. C; mock-treated control cells without restriction endonucleases. Black bars and dark gray bars represent cells with Type IV and Type III nuclei, respectively.

(Figures 6 and 10). Thus, these results indicate that a part of DNA double strand breaks, created by restriction endonucleases generating blunt ends and 5'-protruding ends, requires ATM-dependent DNA repair pathway.

The major pathway responsible for repair of DNA double strand breaks in G1 is DNA-PK-dependent NHEJ [1-6], and our results and others indicated that NHEJ pathway could repair most of the restriction endonuclease-induced DNA double strand breaks irrespective of ATM

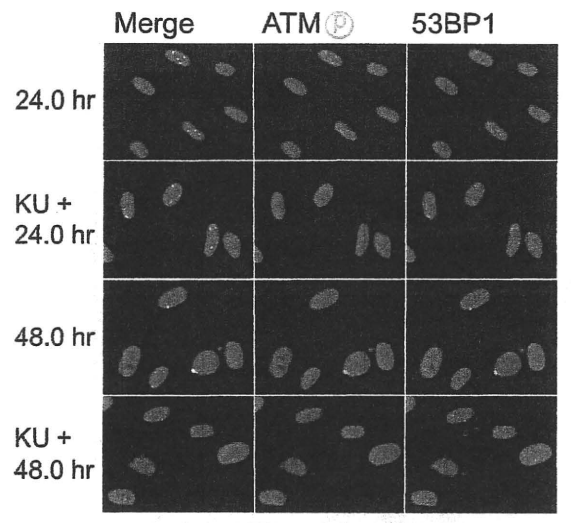

Figure 7 Effect of ATM inhibition on distribution of foci number. Synchronized normal human diploid cells in G1 were electroporated with 100 U of *Pvu* II with or without 20 μM KU55933. The cells were incubated for the time indicated before fixation.

deficiency [37,38]. However, ATM inhibition partly compromised repair of foci, especially, those persisted foci for over 24 hours. According to the previous results, these residual foci possibly represented chromatins with unreparable DNA breaks, DNA breaks refractory for repair, and those harboring mis-rejoined DNA damage [7,50]. Since a part of residual foci gradually reduced in number in the presence of ATM activity, it seems likely that they represent DNA breaks refractory for repair by a conventional NHEJ pathway. We presumed that such slowly-repairing DNA damage required ATM-dependent pathway. The important information was that ATM activity was required for the repair of 5'-protruding and blunt ends, whereas it did not show any role in repair of 3'-protruding DNA double strand breaks. Therefore, it is likely that a part of 5'-protruding and blunt termini requires ATM activity to expose 3'-protruding ends, whose process needs 5' to 3' exonuclease activity.

Then, how does ATM activity regulate end processing? One possibility is that Artemis is involved in this processing. Artemis was the first component, involved in NHEJ pathway, which is phosphorylated by ATM [23,25]. An epistasis-type analysis demonstrated that AT cells and Artemis-defective cells showed identical DNA repair phenotypes [22]. Furthermore, addition of ATM inhibitor to Artemis-defective cells resulted in no additive effect on repair of residual damage. Thus, it was concluded that ATM and Artemis function in the same DNA repair pathway. Artemis has 5' to 3' exonuclease activity towards single stranded DNA, while it also acquires endonuclease activity in the presence of DNA-PK [25,51,52]. Although subsequent studies have demonstrated that DNA-PK is

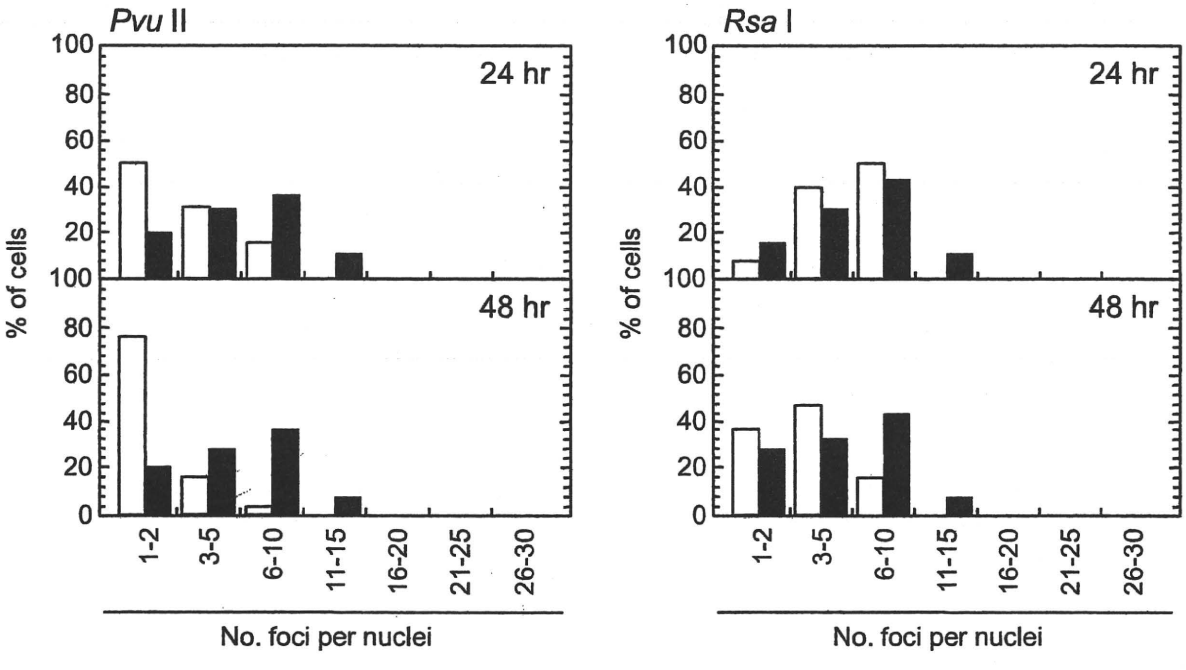

Figure 8 Distribution of foci numbers per nucleus. Synchronized normal human diploid cells in G1 were electroporated with 100 U of *Pvu* II and *Rsa* I with or without 20 μM KU55933. The cells were incubated for 24 or 48 hours after the treatment, and the foci numbers in Type III nuclei were counted. At least 500 nuclei were examined. Black bars: cells treated with KU55933. White bars: cells treated without KU55933.

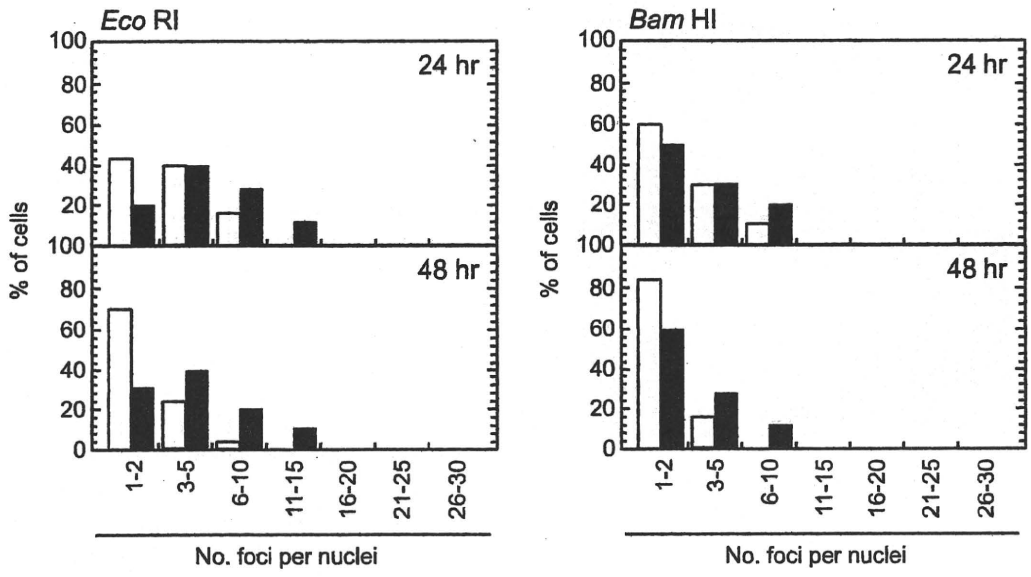

Figure 9 Distribution of foci numbers per nucleus. Synchronized normal human diploid cells in G1 were electroporated with 100 U of *Eco* RI and *Bam* HI with or without 20 μM KU55933. The cells were incubated for 24 or 48 hours after the treatment, and the foci numbers in Type III nuclei were counted. At least 500 nuclei were examined. Black bars: cells treated with KU55933. White bars: cells treated without KU55933.

an essential factor for Artemis activity [51], ATM-dependent phosphorylation was suggested to inhibit regulation of Artemis by DNA-PK-dependent phosphorylation [53]. Therefore, it is possible that ATM regulates exonuclease activity of Artemis involved in end-processing of broken DNA ends. Although we need further investigation, a plausible mechanism is that some residual DNA breaks need processing by Artemis to create the 3'-protruding ends. According to the recent review, the initial step of DNA-PK-dependent NHEJ starts by binding of Ku80/70 heterodimers to the broken ends [6]. In most cases, DNA-PKcs tethers the broken ends by interacting with Ku80/70 heterodimers. But, clustered damage was introduced by restriction endonucleases in a localized area, DNA-PK-dependent pathway can not be functional anymore, and backup repair system takes place. Or, some broken termini might be attacked by endogenous nucleases, which results in incompatible ends. In either case, DNA ends may need processing by Artemis.

Although ATM activity is required for reorganizing heterochromatin through KAP-1 phosphorylation [28], it might not explain the results obtained in this study. If ATM-dependent heterochromatin reorganization was involved in repair of residual foci, ATM inhibition affected repair of residual foci irrespective of the structure of broken ends. However, this assumption was not in agreement with the results, in which the repair of *Pst* I- and *Sph* I-induced damage was insensitive to ATM inhibition. Thus, it is more likely that ATM activity plays a role in activating Artemis-dependent DNA processing a subset of DNA double strand breaks. Although future studies should define the molecular nature of this process, our results suggest that hyper radiosensitivity of AT cells might be explained in part by a defect in this process.

Conclusions

Radiosensitive AT cells showed difficulty to rejoin a small fraction of DNA double strand breaks. Our current study demonstrated that a part of residual blunt and 5'-protruding ends required ATM activity, but repair of residual 3'-protruding ends was not affected by ATM inhibition. Thus, it is concluded that the defect in ATM-dependent DNA repair pathway, which is indispensable for the repair of subsets of residual breaks, could be a cause of increased radiosensitivity of AT cells.

Methods

Cell culture

Normal human diploid fibroblast-like cells [54,55], which derived from embryonic dermal tissue, were cultured in MEM supplemented with 10% fetal bovine serum

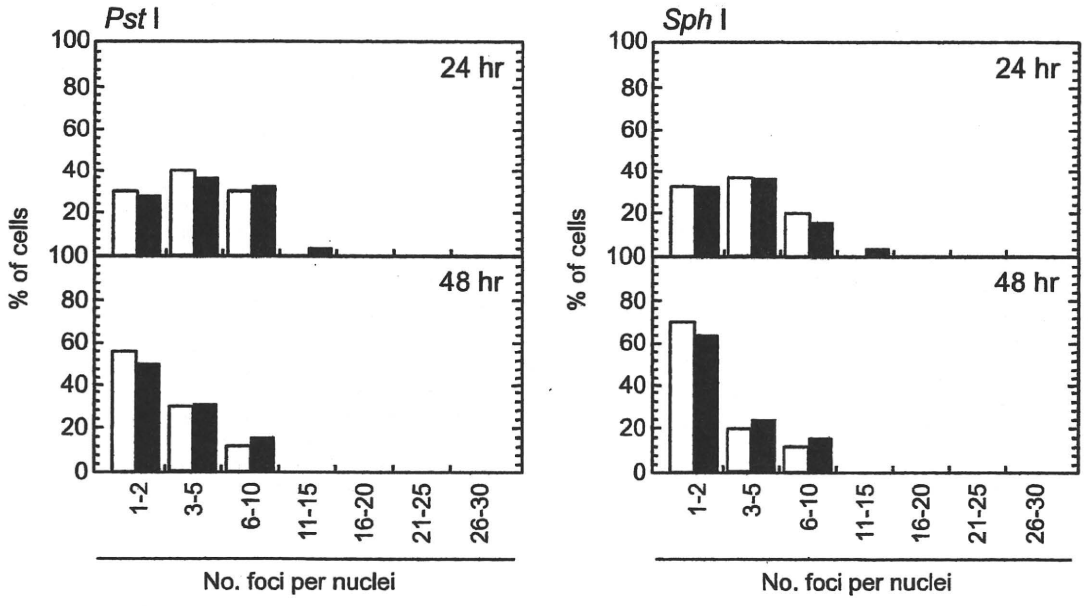

Figure 10 Distribution of foci numbers per nucleus. Synchronized normal human diploid cells in G1 were electroporated with 100 U of *Pst* I and *Sph* I with or without 20 μM KU55933. The cells were incubated for 24 or 48 hours after the treatment, and the foci numbers in Type III nuclei were counted. At least 500 nuclei were examined. Black bars: cells treated with KU55933. White bars: cells treated without KU55933.

(TRACE Bioscience PTY Ltd., Australia). To obtain synchronized cells the cells were subcultured at a high density for days with changing medium every 3 days. After 7 days-synchronization, more than 95% of cells were in G0/G1. The ATM kinase activity was inhibited by a specific inhibitor, KU55933, and 20 μM of KU55933 was administrated 30 min before electroporation. Immediately after electroporation, a fresh medium containing 20 μM of KU55933 was fed, and the cells were cultured at 37°C in a 5% CO_2 incubator until they were fixed. In order to visualize phosphorylated ATM foci and 53 BP1 foci, the cells were incubated for one with a fresh medium without KU55933.

Introduction of restriction endonucleases by electroporation

Synchronized cells were washed with phosphate-buffered saline (PBS) twice, collected by trypsinization and resuspended in PBS at a concentration of 2×10^6/ml. Then, 450 μl of cell suspension was mixed with 50 μl of reaction buffer, and restriction endonucleases were added before electroporation (pulse height and width were 400 V/cm and 1000 msec, respectively). Immediately after electroporation, a fresh medium was fed, and cells were plated onto sterilized 22 × 22 mm cover slips at a density of 5×10^4 cells per slip. The cells were incubated at 37°C in a 5% CO_2 incubator until they were fixed. Restriction endonucleases were obtained from Nippon Gene (Tokyo, Japan).

Immunofluorescence

Cells cultured on coverslips were fixed with 4% formaldehyde for 10 min, permeabilized with 0.5% Triton X-100 for 5 min, and were washed extensively with phosphate-buffered saline (PBS). Fixation and permeabilization were performed on ice. The primary antibodies were diluted in 100 μl of TBS-DT (20 mM Tris-HCl, pH7.6, 137 mM NaCl, containing 50 mg/ml skim milk and 0.1% Tween-20), and the antibodies were applied on the coverslips. The samples were incubated for 2 hours in a humidified CO_2 incubator at 37°C. Then, the primary antibodies were washed with PBS, and Alexa488-labelled anti-mouse or Alexa594-labelled anti-rabbit IgG antibodies (Molecular Probes, Inc., OR) were added. The coverslips were incubated for 1 hour in a humidified CO_2 incubator at 37°C, washed with PBS, and counterstained with 0.1 mg/ml of DAPI. The samples were examined with a F3000B fluorescence microscope (Leica, Tokyo). Digital images were captured and the images were analyzed by FW4000 software (Leica, Tokyo). In order to quantify the fluorescence intensity, green dot-like signals were marked, and the sum of the pixel intensity within the marked area was calculated by FW4000 software. The primary antibodies used in this study were mouse anti-

phosphorylated ATM at serine 1981 monoclonal antibody (Clone 10 H11.E12, Rockland, Gilbertsville, PA), rabbit anti-53 BP1 polyclonal antibody (A300-272 A, BETHYL, Montgomery, TX), rabbit anti-phosphorylated NBS1 at serine 343 polyclonal antibody (A300-189 A, BETHYL, Montgomery, TX), rabbit anti-phosphorylated histone H2AX at serine 139 polyclonal antibody (A300-081 A, BETHYL, Montgomery, TX), and rabbit anti-phosphorylated 53 BP1 at serine 1778 polyclonal antibody (2675, Cell Signaling Technology Japan, Tokyo).

Additional material

Additional file 1 Colocalization of the foci of phosphorylated proteins. Synchronized normal human diploid cells in G1 were electroporated with *Pvu* II (100 U) as described in METHODS. The cells were incubated for 12 hours before fixation.

Competing interests

The authors declare that they have no competing interests.

Authors' contributions

KS conceived of the study, carried out the immunoflorescence study, and drafted the manuscript. MT carried out the immunoflorescence study and performed the statistical analysis. YO participated in the design of the study. MY participated in the design of the study and carried out the immunoflorescence study. MS participated in the design of the study. SY helped to draft the manuscript. All authors read and approved the final manuscript.

Acknowledgements

This study was supported in part by the Global Center Of Excellence (GCOE) Program and Grant-in-Aid for Scientific Research from the Ministry of Education, Culture, Sports, Science and Technology, Japan.

Author Details

Atomic Bomb Disease Institute, Nagasaki University Graduate School of Biomedical Sciences, 1-12-4 Sakamoto, Nagasaki 852-8523, Japan

Received: 26 January 2010 Accepted: 26 May 2010
Published: 26 May 2010

References

1. Burma S, Chen BP, Chen DJ: **Role of non-homologous end joining (NHEJ) in maintaining genomic integrity.** *DNA Repair* 2006, **5**:1042-1048.
2. Sonoda E, Hochegger H, Saberi A, Taniguchi Y, Takeda S: **Differential usage of non-homologous end-joining and homologous recombination in double strand break repair.** *DNA Repair* 2006, **5**:1021-1029.
3. Wyman C, Kanaar R: **DNA double-strand break repair: all's well that ends well.** *Annu Rev Genet* 2006, **40**:363-383.
4. Jeggo P, Lavin MF: **Cellular radiosensitivity: How much better do we understand it?** *Int J Radiat Biol* 2009, **85**:1061-1081.
5. Lisby M, Rothstein R: **Choreorgaphy of recombination proteins during the DNA damage response.** *DNA Repair* 2009, **8**:1068-1076.
6. Mahaney BL, Meek K, Lees-Miller SP: **Repair of ionizing radiation-induced DNA double-strand breaks by non-homologous end-joining.** *Biochem J* 2009, **417**:639-650.
7. Agarwal S, Tafel AA, Kanaar R: **DNA double-strand break repair and chromosome translocations.** *DNA Repair* 2006, **5**:1075-1081.
8. Jeggo P, Lobrich M: **Contribution of DNA repair and cell cycle checkpoint arrest to the maintainance of genomic stability.** *DNA Repair* 2006, **5**:1192-1198.
9. Weinstock DM, Brunet E, Jasin M: **Induction of chromosomal translocations in mouse and human cells using site-specific endonucleases.** *J Natl Cancer Inst Monogr* 2008, **39**:20-24.
10. Bartek J, Bartkova J, Lukas J: **DNA damage signalling guards against activated oncogenes and tumour progression.** *Oncogene* 2007, **26**:7773-7779.
11. Harper JW, Elledge SJ: **The DNA damage response: ten years after.** *Mol Cell* 2007, **28**:739-745.
12. Shiloh Y: **ATM and related proteins kinases: safeguarding genome integrity.** *Nat Rev Cancer* 2003, **3**:155-168.
13. Kitagawa R, Kastan MB: **The ATM-dependent DNA damage signaling pathway.** *Cold Spring Harb Symp Quant Biol* 2005, **70**:99-109.
14. Lavin MF: **Ataxia-telangiectasia: from a rare disorder to a paradigm for cell signalling and cancer.** *Nat Rev Mol Cell Biol* 2008, **9**:759-769.
15. Bakkenist CJ, Kastan MB: **DNA damage activates ATM through intermolecular autophosphorylation and dimer dissociation.** *Nature* 2003, **421**:499-506.
16. Jackson SP, Bartek J: **The DNA-damage response in human biology and disease.** *Nature* 2009, **461**:1071-1078.
17. Jackson SP: **The DNA-damage response: new molecular insights and new approaches to cancer therapy.** *Biochem Soc Trans* 2009, **37**:483-494.
18. Pollard JM, Gatti RA: **Clinical radiation sensitivity with DNA repair disorders: an overview.** *Int J Radiat Oncol Biol Phys* 2009, **74**:1323-1331.
19. Foray N, Priestley A, Alsbeih G, Badie C, Capulas EP, Arlett CF, Malaise EP: **Hypersensitivity of ataxia-telangiectasia fibroblasts to ionizing radiation is associated with a repair deficiency of DNA double-strand breaks.** *Int J Radiat Biol* 1997, **72**:271-283.
20. Jeggo PA, Carr AM, Lehmann AR: **Splitting the ATM: distinct repair and checkpoint defects in ataxia-telangiectasia.** *Trends Genet* 1998, **14**:312-316.
21. Kuhne M, Riballo E, Rief M, Rothkamm K, Jeggo PA, Lobrich M: **A double-strand break repair defect in ATM-deficient cells contributes to radiosensitivity.** *Cancer Res* 2004, **64**:500-508.
22. Riballo E, Kuhne M, Rief N, Doherty A, Smith GCM, Recio MJ, Reis C, Dahm K, Fricke A, Krempler A, Parker AR, Jackson SP, Gennery A, Jeggo PA, Lobrich M: **A pathway of double-strand break rejoining dependent upon ATM, Artemis, and proteins locating to γ-H2AX foci.** *Mol Cell* 2004, **16**:715-724.
23. Jeggo PA, Lobrich M: **Artemis links ATM to double strand break rejoining.** *Cell Cycle* 2005, **4**:359-362.
24. Lobrich M, Jeggo PA: **Harmonising the response to DSBs: a new string in the ATM bow.** *DNA Repair* 2005, **4**:749-759.
25. Dahm K: **Functions and regulation of human Artemis in double strand break repair.** *J Cell Biochem* 2007, **100**:1346-1351.
26. Poinsignon C, de Chasseval R, Soubeyrand S, Moshous D, Fischer A, Hache RJG, de Villartay JP: **Phosphorylation of Artemis following irradiation-induced DNA damage.** *Eur J Immunol* 2004, **34**:3146-3155.
27. Zhang X, Succi J, Feng Z, Prithivirasingh S, Story MD, Legersky R: **Artemis is a phosphorylation target of ATM and ATR and is involved in the G2/M DNA damage checkpoint response.** *Mol Cell Biol* 2004, **24**:9207-9220.
28. Goodarzi AA, Noon AT, Deckbar D, Ziv Y, Shiloh Y, Lobrich M, Jeggo PA: **ATM signaling facilitates repair of DNA double-strand breaks associated with heterochromatin.** *Mol Cell* 2008, **31**:167-177.
29. Kruhlak MJ, Celeste A, Dellaire G, Fernadez-Capetillo O, Muller WG, McNally JG, Bazett-Jones DP, Nussenzweig A: **Changes in chromatin structure and mobility in living cells at sites of DNA double-strand breaks.** *J Cell Biol* 2006, **172**:823-834.
30. Ball AR, Yokomori K: **Revisiting the role of heterochromatin protein 1 in DNA repair.** *J Cell Biol* 2009, **185**:573-575.
31. Cowell IG, Sunter NJ, Singh PB, Austin CA, Durkacz BW, Tilby MJ: **Gamma-H2AX foci form preferentially in euchromatin after ionising-radiation.** *PLoS ONE* 2007, **2**:e1057. 10.1371/journal.pone.0001057
32. Murga M, Jaco I, Fan Y, Soria R, Martinez-Pastor B, Cuadrado M, Yang SM, Blasco MA, Skoultchi AI, Fernandez-Capetillo O: **Global chromatin compaction limits the strength of the DNA damage response.** *J Cell Biol* 2007, **178**:1101-1108.
33. Goodarzi AA, Noon AT, Jeggo PA: **The impact of heterochromatin on DSB repair.** *Biochem Soc Trans* 2009, **37**:569-576.
34. Ayoub N, Jeyasekharan AD, Bernal JA, Venkitaraman AR: **HP1-β mobilization promotes chromatin changes that initiate the DNA damage response.** *Nature* 2008, **453**:682-686.
35. Fernadez-Capetillo O, Nussenzweig A: **ATM breaks into heterochromatin.** *Mol Cell* 2008, **31**:303-304.

36. Winegar RA, Phillips JW, Youngblom JH, Morgan WF: **Cell electroporation is a highly efficient method for introducing restriction endonucleases into cells.** *Mutat Res* 1989, **225**:49-53.
37. Liu N, Bryant PE: **Response of ataxia telangiectasia cells to restriction endonuclease induced DNA double-strand breaks: I. Cytogenetic characterization.** *Mutagenesis* 1993, **8**:503-510.
38. Liu N, Bryant PE: **Enhanced chromosomal response of ataxia-telangiectasia cells to specific types of DNA double-strand breaks.** *Int J Radiat Biol* 1994, **66(Supple 6)**:115-121.
39. Bryant PE: **Use of restriction endonucleases to study relationships between DNA double-strand breaks, chromosomal aberrations and other end-points in mammalian cells.** *Int J Radiat Biol* 1988, **54**:869-890.
40. Bryant PE, Johnston PJ: **Restriction-endonuclease-induced DNA double-strand breaks and chromosomal aberrations in mammalian cells.** *Mutat Res* 1993, **299**:289-296.
41. Ortiz T, Pinero J, Cortes F: **Chromosome damage induced by combined treatments with restriction endonucleases introduced into CHO cells by single or double electroporation.** *Mutat Res* 1995, **327**:161-169.
42. Rogakou EP, Boon C, Redon C, Bonner WM: **Megabase chromatin domains involved in DNA double-strand breaks in vivo.** *J Cell Biol* 1999, **146**:905-915.
43. Olive PL: **Detection of DNA damage in individual cells by analysis of histone H2AX phosphorylation.** *Methods Cell Biol* 2004, **75**:355-373.
44. FitzGerald JE, Grenon M, Lowndes NF: **53 BP1: function and mechanism of focal recruitment.** *Biochem Soc Trans* 2009, **37**:897-904.
45. Fernandez-Capetillo O, Lee A, Nussenzweig M, Nussenzweig A: **H2AX: the histone guardian of the genome.** *DNA Repair* 2004, **3**:959-967.
46. Bonner WM, Redon CE, Dickey JS, Nakamura AJ, Sedelnikova OA, Solier S, Pommier Y: **GammaH2AX and cancer.** *Nat Rev Cancer* 2008, **8**:957-967.
47. Kinner A, Wu W, Staudt C, Iliakis G: **Gamma-H2AX in recognition and signaling of DNA double-strand breaks in the context of chromatin.** *Nucleic Acids Res* 2008, **36**:5678-5694.
48. Hickson I, Zhao Y, Richardson CJ, Green SJ, Martin NM, Orr AI, Reaper PM, Jackson SP, Curtin NJ, Smith GC: **Identification and characterization of a novel and specific inhibitor of the ataxia-telangiectasia mutated kinase ATM.** *Cancer Res* 2004, **64**:9152-9159.
49. Huyen Y, Zgheib O, Ditullio RA Jr, Gorgoulis VG, Zacharatos P, Petty TJ, Sheston EA, Mellert HS, Stavridi ES, Halazonetis TD: **Methylated lysine 79 of histone H3 targets 53 BP1 to DNA double-strand breaks.** *Nature* 2004, **432**:406-411.
50. Kato TA, Okayasu R, Bedford JS: **Signatures of DNA double strand breaks produced in irradiated G1 and G2 cells persist into mitosis.** *J Cell Physiol* 2009, **219**:760-765.
51. Goodarzi AA, Yu Y, Riballo E, Douglas P, Walker SA, Ye R, Harer C, Marchetti C, Morrice N, Jeggo PA, Lees-Miller SP: **DNA-PK autophosphorylation facilitates Artemis endonuclease activity.** *The EMBO J* 2006, **25**:3880-3889.
52. Yannone SM, Khan IS, Zhou RZ, Zhou T, Valerie K, Povirk LF: **Coordinate 5' and 3' endonucleolytic trimming of terminally blocked blunt DNA double-strand break ends by Artemis nuclease and DNA-dependent protein kinase.** *Nucleic Acids Res* 2008, **36**:3354-3365.
53. Beucher A, Birraux J, Tchouandong L, Barton O, Shibata A, Conrad S, Goodarzi AA, Krempler A, Jeggo PA, Lobrich M: **ATM and Artemis promote homologous recombination of radiation-induced DNA double-strand breaks in G2.** *The EMBO J* 2009, **28**:3413-3427.
54. Suzuki K, Okada H, Yamauchi M, Oka Y, Kodama S, Watanabe M: **Qualitative and quantitative analysis of phosphorylated ATM foci induced by low dose ionizing radiation.** *Radiat Res* 2006, **165**:499-504.
55. Watanabe M, Suzuki M, Suzuki K, Nakano K, Watanabe K: **Effect of multiple irradiation with low doses of gamma-rays on morphological transformation and growth ability of human embryo cells in vitro.** *Int J Radiat Biol* 1992, **62**:711-718.

doi: 10.1186/2041-9414-1-4
Cite this article as: Suzuki *et al.*, Requirement of ATM-dependent pathway for the repair of a subset of DNA double strand breaks created by restriction endonucleases *Genome Integrity* 2010, **1**:4